Western equatorial Pacific deep water carbonate chemistry during the Last Glacial Maximum and deglaciation: Using planktic foraminiferal Mg/Ca to reconstruct sea surface temperature and seafloor dissolution

Jennifer Fehrenbacher[1] and Pamela Martin[1]

Received 6 August 2010; revised 9 March 2011; accepted 25 March 2011; published 30 June 2011.

[1] We present a reconstruction of deep-water carbonate saturation state (ΔCO_3^{2-}) in the western equatorial Pacific for the Last Glacial Maximum (LGM) and deglaciation based on changes in the Mg/Ca ratio of planktic foraminifers with increased water depth. Our data suggest there have been changes in bottom water ΔCO_3^{2-} over the past 25,000 years at water depths as shallow as 1.6 km. The ΔCO_3^{2-} reconstruction for the LGM suggests ΔCO_3^{2-} was similar or slightly higher than modern values between 1.6 and 2.0 km, shifting sharply to lower values (an average ~30 μmol/kg lower) below 2.5 km. The shift in chemistry between 2.0 and 2.5 km supports a hypothesis that Pacific overturning circulation occurred deeper during the LGM with a slightly more ventilated water mass above 2.0 km. The data are not consistent with enhanced preservation in this region of the deep Pacific at depths greater than 2.5 km, suggesting that the long-held view of better preservation throughout the glacial deep Pacific must be reevaluated. For the deglaciation, we have evidence of a ΔCO_3^{2-} maximum that suggests enhanced deglacial preservation between 1.6 and 4.0 km in comparison to the Holocene and the LGM. The deglacial ΔCO_3^{2-} was as much as 28 μmol/kg higher than modern between 1.6 and 4.0 km. Results suggest carbonate burial rates were 1.5 times greater during the deglacial than the over the past 5 kyr.

Citation: Fehrenbacher, J., and P. Martin (2011), Western equatorial Pacific deep water carbonate chemistry during the Last Glacial Maximum and deglaciation: Using planktic foraminiferal Mg/Ca to reconstruct sea surface temperature and seafloor dissolution, *Paleoceanography*, *26*, PA2225, doi:10.1029/2010PA002035.

1. Introduction

[2] The pCO_2 of the atmosphere has varied between 180 and 280 ppm over glacial and interglacial cycles. Given the large reservoir of carbon exchangeable on glacial-interglacial time scales, the ocean is a viable driver for such changes in pCO_2, though the mechanism behind this variability remains elusive (see *Archer et al.* [2000] for a review). If the ocean was at least partly responsible for changes in atmospheric pCO_2 we would expect to see variability in deep water carbonate ion concentration, $[CO_3^{2-}]$, and also preservation of calcite sediments, coincident with changes in atmospheric pCO_2. The $[CO_3^{2-}]$ of the deep ocean is set at deep-water sources and is modified through the process of chemical aging. The combination of surface processes and respiration in the deep sea are the primary reason for the low $[CO_3^{2-}]$ of the deep Pacific, which has accumulated more dissolved inorganic carbon (DIC) through chemical aging than the more recently ventilated deep Atlantic that has higher $[CO_3^{2-}]$. Interpreting changes in the $[CO_3^{2-}]$ of the deep sea in the past is complicated because both surface and deep water processes must be taken into account. Nonetheless, changes in $[CO_3^{2-}]$ of deep water can be used to test hypotheses regarding changes in both the carbon cycle and ocean circulation through time.

[3] Over the last decade several approaches have been used to reconstruct glacial to interglacial changes in deep ocean $[CO_3^{2-}]$ (or ocean pH) [*Anderson and Archer*, 2002; *Broecker and Clark*, 2001a, 2001b, 2003; *Marchitto et al.*, 2005; *Yu and Elderfield*, 2007; *Hönisch and Hemming*, 2005]. *Broecker and Clark* [2001a, 2001b, 2003] used changes in planktic foraminiferal shell weights to quantify changes in $[CO_3^{2-}]$ with increasing water depth in the tropical Atlantic and tropical Pacific. The shell weight proxy, though complicated by enhanced shell growth during glacial periods, suggests enhanced preservation in the Atlantic during the LGM and a steeper $[CO_3^{2-}]$ gradient in the Pacific. *Anderson and Archer* [2002] used planktic foraminiferal shell assemblages to reconstruct $[CO_3^{2-}]$ during the LGM in the Atlantic, Pacific, and Indian Ocean basins and found little change in the $[CO_3^{2-}]$ gradient during the LGM in comparison to today. *Marchitto et al.* [2005] showed that the Zn/Ca ratio

[1]Department of Geophysical Sciences, University of Chicago, Chicago, Illinois, USA.

0883-8305/11/2010PA002035

in benthic foraminifera varies as a function of the ΔCO_3^{2-} of bottom waters and used this relationship to quantify changes in the ΔCO_3^{2-} of the tropical eastern Pacific during the deglaciation and LGM. The results suggested the LGM ΔCO_3^{2-} was similar to or slightly lower than the modern Pacific and the ΔCO_3^{2-} during the deglaciation was 20–30 μmol/kg higher than modern. The results of these studies vary and highlight the need for additional proxies and further investigation of deep ocean carbonate chemistry since the LGM.

[4] We present results of a deep-water carbonate ion reconstruction of the tropical Pacific Ocean based on planktic foraminiferal Mg/Ca ratios. The Mg/Ca ratio in foraminiferal calcite is an established and widely used paleotemperature proxy, but is also affected by dissolution [*Anand et al.*, 2003; *Hastings et al.*, 1998; *Katz*, 1973; *Lea et al.*, 1999, 2000; *Mashiotta et al.*, 1999; *McConnell and Thunell*, 2005; *McKenna and Prell*, 2004; *Nürnberg and Groeneveld*, 2006; *Nürnberg et al.*, 1996; *Oomori et al.*, 1987; *Regenberg et al.*, 2006]. Dissolution lowers the planktic foraminiferal Mg/Ca ratio, which results in an underestimation of sea surface temperatures if not accounted for in the temperature equation [*Brown and Elderfield*, 1996; *de Villiers*, 2003; *Dekens et al.*, 2002; *Regenberg et al.*, 2006]. Dissolution can take place in the water column [*Peterson*, 1966], on the seafloor, and in the sediment [*Archer et al.*, 1989]. A significant factor in controlling dissolution is the calcite saturation state of deep waters (ΔCO_3^{2-}), which is the relative difference between the in situ carbonate ion concentration ($[CO_3^{2-}]_{in\ situ}$) and the saturation carbonate ion concentration ($[CO_3^{2-}]_{sat}$). Although the mechanism is not fully understood, the decrease in the Mg/Ca ratio of several planktic foraminifers has been shown via core top calibrations to vary quantitatively with changes in deep water calcite saturation state [*Dekens et al.*, 2002]. We exploit this dissolution effect on the Mg/Ca ratio to reconstruct changes in ΔCO_3^{2-} during the LGM and deglaciation. The results provide further insight into the carbonate chemistry and glacial circulation pattern of the deep tropical Pacific since the LGM.

2. Approach and Samples

[5] Several investigators have quantitatively determined the effect of dissolution on the Mg/Ca ratio of different species of planktic foraminifers [*Rosenthal and Lohmann*, 2002; *Dekens et al.*, 2002]. In a previous study we used the calibration data set of *Dekens et al.* [2002] and slightly modified calibration equations based on deep water ΔCO_3^{2-} to reconstruct carbonate ion concentration in the western tropical Atlantic Ocean during the LGM [*Fehrenbacher et al.*, 2006]. For this study, we apply the same concept to a set of cores obtained from a depth transect (1.6–4.0 km) in the western tropical Pacific on the Ontong Java Plateau (Figure 1 and Table 1).

[6] The cores used in this study, giant gravity cores collected on cruise 91-9 of R/V *Moana Wave*, are low sedimentation rate cores from the Ontong Java Plateau located in the western warm pool of the tropical Pacific, a region of low productivity [*Berger*, 1978]. Drawbacks of using these low sedimentation cores with older core top ages (see section 3.2 for age model details), are that (1) we cannot reconstruct the modern so instead focus on the Holocene as our youngest time slice (see section 3.3 for details regarding the time slices and data used in our reconstructions) and (2) bioturbation has likely attenuated the glacial-interglacial signal thus it is unlikely we capture the full signal or exact timing of changes in carbonate ion concentration. In addition, the intensity of bioturbation may be different among the cores, which could introduce error in the reconstructions. (Note that we summarize the implications of bioturbation on our reconstructions in section 6.6.) All of the cores have moderately well defined glacial–interglacial $\delta^{18}O$ amplitudes, implying that bioturbation has not obliterated our signal. We expect changes in the carbonate system to be slow enough to be captured in these slowly accumulating cores. Additionally, the study location is also convenient for comparison with previously published carbonate ion reconstructions for the Ontong Java Plateau, specifically, and the deep equatorial Pacific more generally [*Anderson and Archer*, 2002; *Broecker and Clark*, 2001a, 2001b, 2003; *Marchitto et al.*, 2005].

[7] An advantage of this site for investigating bottom water $[CO_3^{2-}]$, relative to sites that may underlie areas of higher productivity, is that there is a smaller offset between the bottom water $[CO_3^{2-}]$ and the $[CO_3^{2-}]$ in pore waters in these low sedimentation rates cores with low organic carbon content, thus the influence of dissolution in the sediment is small (for further discussion, see *Broecker* [2008]). Pore water oxygen profiles and benthic chamber experiments from this region suggest metabolic CO_2 production occurs in cores located above and below the lysocline [*Jahnke et al.*, 1994; *Hales*, 2003]. However, measurements suggest metabolic CO_2 production occurs near the sediment/water interface, which allows a greater fraction of the CO_2 produced to diffuse out of the pore water minimizing the reaction with calcite [*Hales*, 2003]. That we have evidence of better preservation during the deglacial relative to the modern in the shallowest core at 1.6 km implies that there is some dissolution above the lysocline during the Holocene, which is likely to be reflective of pore dissolution. We note that the interpretation of our results, and the results obtained from any paleoproxy that is affected by dissolution in the sediment, may be further complicated if there has been a significant change in the delivery of organic carbon to the sediment over the time scale of our study.

[8] The cores used in this study are closely spaced and contain planktic foraminifers that likely calcified under similar sea surface and thermocline conditions; thus, we assume the planktic foraminifers should have had similar Mg/Ca ratios, set by the calcification temperature, as they fell to the seafloor. Modern upper water column temperature profiles show that the modern upper water column temperatures vary by less than 0.5°C at any given water depth above the sites for the suite of cores used here (Figure 1b). A difference in calcification temperature, 0.5°C, could result in a small shift in the carbonate ion reconstructions (~4 μmol/kg), which we take into consideration in interpreting our results. The shells settled on the seafloor at different depths where they experienced different intensities of dissolution due to the difference in bottom water calcite saturation state. We use the decrease in the Mg/Ca ratio with increased water depth to determine temporal changes in the carbonate ion gradient (in terms of ΔCO_3^{2-}) during the Holocene, deglaciation, and LGM. We introduce a new approach here and constrain the calcification temperature estimates (which constrains the

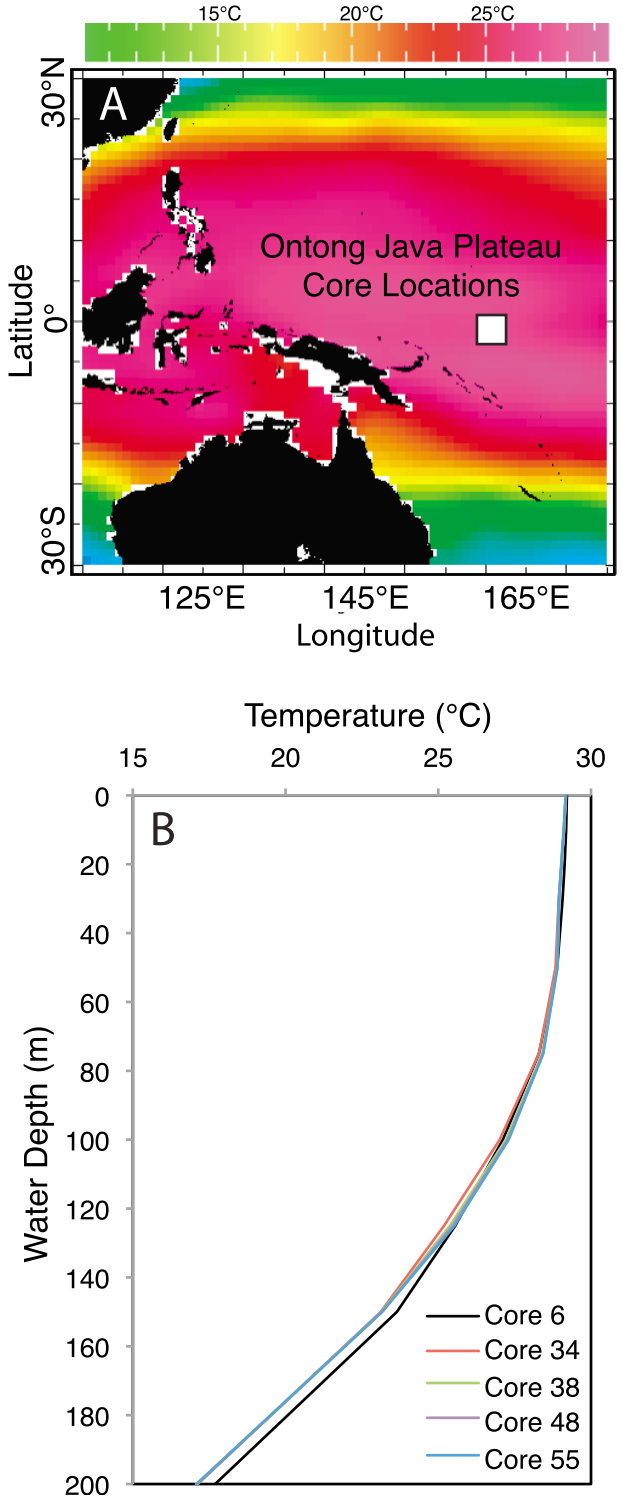

Figure 1. (a) Regional map that details surface temperatures and study location (white box). (b) Also included are the upper water column temperature profiles for each of the cores [from *Levitus and Boyer*, 1994]. The latitude and longitude used to generate the profiles is detailed in Table 1. The temperature profiles are similar to within less than 0.5°C. This offset could result in slight offsets among the initial Mg/Ca ratios recorded in the shells and generate an offset in the reconstructions of ~4 μmol/kg between each of the cores.

initial Mg/Ca ratio) in the shallow core and the carbonate ion concentration in situ ($[CO_3^{2-}]_{in\ situ}$) in all cores using two species that have different sensitivities to temperature and dissolution.

3. Stratigraphy

3.1. Stratigraphic Control

[9] Age models, developed as part of this study, are based on radiocarbon and oxygen isotope measurements. Radiocarbon was measured on core top intervals (0–2 cm) (with the exception of core MW91-9 55 in which the 2–4 cm interval was chosen due to insufficient remaining sample for analysis) and intervals estimated to be within the LGM. In the shallowest core (MW91-9 6GGC, 1.6 km), a deglacial interval was also analyzed (Table S1 in the auxiliary material).[1] For each radiocarbon analysis, 0.5–1 mg of shells of the species *G. sacculifer* were picked from coarse fraction (>250 μm). Radiocarbon analyses were performed at Lawrence Livermore National Laboratory Center for Accelerator Mass Spectrometry. Radiocarbon ages were converted to calendar age following *Fairbanks et al.* [2005] using a regional reservoir effect correction of 256 years (http://radiocarbon.LDEO.columbia.edu) [*Butzin et al.*, 2005].

[10] Stable isotopes were measured in the same sample intervals used for Mg/Ca analysis on *N. dutertrei* in all five cores, *G. ruber* in all cores with exception of the deepest core and *G. sacculifer* in cores MW91-9 6GGC and 48GGC (Figures 2d–2f). The *G. ruber* data for MW91-9 48 are from D. Lea and M. J. Coombs (unpublished data, 2003). Approximately 5–15 shells were picked from the 250–355 μm size fraction for each stable isotope measurement. Analyses were performed at the University of California, Santa Barbara using a GV Isoprime Isotope Ratio Mass Spectrometer in dual inlet mode. The analytical precision of the measurements is ±0.08‰ for $\delta^{18}O$ and ±0.05‰ for $\delta^{13}C$ determined by replicate analysis of NBS-19 standard and a house carbonate standard.

3.2. Age Model Construction

[11] The radiocarbon ages of the core tops vary with depth from 4400 to 7000 calendar years (Table S1). The different core top ages likely reflect a combination of bioturbation and preferential dissolution [*Barker et al.*, 2007; *Berger*, 1970; *Broecker et al.*, 1999]. Oxygen isotopes and radiocarbon ages are in general agreement with respect to the depth of the LGM, ranging from 33 to 45 cm in this suite of cores. Age constraints imply a sedimentation rate of 1 to 2 cm/kyr, similar to other cores from the Ontong Java Plateau [*Berger and Killingley*, 1982; *Shackleton and Opdyke*, 1977] (Table 1). We note that these cores are giant gravity cores, which typically are compacted during coring, thus the true sedimentation rate is likely greater than the implied rate. A box core from this region suggests a sedimentation rate of 2–3 cm/year (Core MW91-9 36BC; 2.3 km) [*Barker et al.*, 2007].

[12] The $\delta^{18}O$ values show a glacial to interglacial negative shift (hereafter referred to as $\Delta\delta^{18}O$) of ~1.2‰ for *G. ruber* in all 4 cores. The $\delta^{18}O$ values for *N. dutertrei*

[1] Auxiliary materials are available in the HTML. doi:10.1029/2010PA002035.

Table 1. Core Locations, Water Depth, and Sea Surface Temperatures of Cores Used in This Study[a]

Core	Latitude	Longitude	Water Depth (m)	SST (°C)	Sedimentation Rate (cm/kyr)	Latitude/Longitude Used for T. Profile[b]
MW91-9 6GGC	2°12.54′S	156°57.9′E	1625	29.3	1.5	2.0°S, 157.5°E
MW91-9 34GGC	0°29.31′S	157°50.2′E	2022	29.3	1.6	0.5°S, 157.5°E
MW91-9 38GGC	0°0.35′N	159°22.0′E	2456	29.1	2.1	0.5°S, 159.5°E
MW91-9 48GGC	0°4.47′S	161°0.2′E	3397	29.1	2.3	0.5°S, 161.5°E
MW91-9 55GGC	0°0.87′S	161°46.4′E	4024	29.1	1.2	0.5°S, 161.5°E

[a]Modern annual average sea surface temperatures are from *Levitus and Boyer* [1994]. Sedimentation rates were derived from stratigraphies developed for this study.
[b]Latitude and longitude used to generate depth profiles (Figure 1) for each of the cores from *Levitus and Boyer* [1994].

show a glacial to interglacial negative shift of 1.2‰–1.9‰, in the suite of cores (spanning 1.6 to 4.0 km). The $\Delta\delta^{18}O$ values are within the range of other published $\Delta\delta^{18}O$ values from the western equatorial Pacific (0.9–1.7‰) [*Berger et al.*, 1983; *Broecker*, 1986; *de Garidel-Thoron et al.*, 2007; *Herguera*, 1994; *Labeyrie et al.*, 1992; *Lea et al.*, 2000; *Martinet et al.*, 1997]. We attribute the small $\Delta\delta^{18}O$ amplitude of the deepest core (1.2‰) to the combination of the lowest sedimentation rate of this core among the suite of cores used in this study (1.2 cm/1000 years compared to 1.6 to 2.3 cm/1000 years) coupled with bioturbation and dissolution. Age offsets in excess of 2000 years among different species often exist in low sedimentation rate cores due to bioturbation and dissolution [*Barker et al.*, 2007].

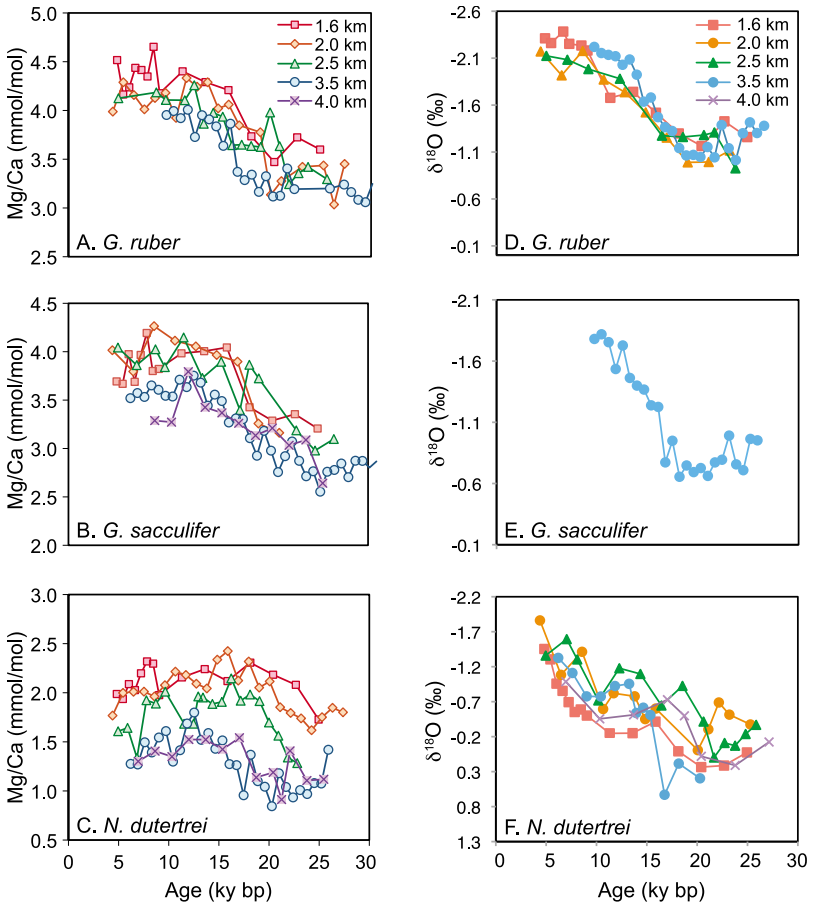

Figure 2. (a–c) Mg/Ca versus age and (d–f) oxygen isotopes versus age grouped by species. *G. ruber* (Figure 2a) and *G. sacculifer* (Figure 2b) show a small decrease in the Mg/Ca ratio with increased water depth relative to the Holocene-LGM change in Mg/Ca. *N. dutertrei* (Figure 2c) show a large decrease in Mg/Ca with increased core depth relative to the entire Holocene-LGM change in Mg/Ca. The decrease with depth is greater during the LGM than modern. The Mg/Ca of *N. dutertrei* increases into the deglaciation then decreases to modern values. Note that there are different Mg/Ca ranges for each species. The legend in Figure 2a corresponds to Figures 2a–2c, and the legend in Figure 2d corresponds to Figures 2d–2f.

G. sacculifer radiocarbon ages were used for the age models, however, *N. dutertrei* Mg/Ca results are used for the LGM and deglacial reconstructions. We discuss the effect of potential errors in our age models on the carbonate ion reconstructions in section 6.6.2.

3.3. Samples Used for the Time Slice Reconstructions

[13] We determine past carbonate ion gradients for three time slices: the Holocene (for comparison to the modern gradient), the deglaciation, and the LGM. For the Holocene reconstruction, we took an average of the intervals of Holocene age (4.4 through 10 ka). The deglacial time slice coincides with a Mg/Ca peak for *N. dutertrei* and the presence of pteropods in the shallow three cores. The age model for the shallow core places the interval with the highest Mg/Ca ratio and the greatest number of pteropods at ~14 ka. The intervals used for the deglacial reconstructions were those with the highest Mg/Ca ratio (averaged with one sample above and below). The intervals with the highest Mg/Ca ratio generally coincided with the intervals ~14 ka. For the LGM, we chose the sample closest to 21 ka following our age models, and use the Mg/Ca of this interval averaged with one interval above and below.

4. Methods: Mg/Ca Measurements

[14] We analyzed Mg/Ca in three species of planktic foraminifers: *G. ruber, G. sacculifer* and *N. dutertrei*. Approximately 50 shells of *N. dutertrei* and *G. sacculifer* and 50–70 *G. ruber* shells were picked from the 250–355 size fraction to yield two analyses. For small samples, 0.35–0.45 mg of shells (~30) were gently crushed between glass plates and placed into one vial. For samples abundant enough for duplicate measurements, ~0.7–1.0 mg of shells were gently crushed between glass plates, homogenized with a dry brush, and separated into two vials. Samples were loaded into vials in a Class-100 clean room. Samples were prepared in a side-ventilated Class-100 flow hood following the standard foraminiferal cleaning protocol without the DTPA step [*Martin and Lea*, 2002; after *Boyle and Keigwin*, 1985].

[15] Samples were analyzed at the University of California, Santa Barbara using the method originally developed for quadrupole ICP-MS [*Lea and Martin*, 1996], modified for the magnetic sector instrument (Element II HR ICP-MS). Samples were analyzed for a suite of minor and trace constituents including barium, aluminum, iron, sodium, and manganese. High Al and/or Fe in planktic foraminiferal samples are indicative of contamination from sediments whereas high Na may indicate contamination from cleaning. Elevated Mn suggests samples may be contaminated with postdepositional authigenic manganese oxides, which may also skew the Mg/Ca ratio [*Boyle*, 1983; *Martin and Lea*, 2002]. Samples with a final size <10 μg were rejected. In addition, 22 samples (~3%) were rejected due to anomalously high Al, Fe, and/or Na. Seven samples (~1%) were rejected for meeting the requirements for outliers; their Mg/Ca ratios were greater than 2σ higher than average of adjacent samples. Six of those seven samples were cleaned and analyzed on the same day and five of the samples that met the outlier test had repeat data splits with lower Mg/Ca ratios, suggesting a systematic analytical problem on that day. Precision of measurements estimated from the standard deviation of replicate analysis of a consistency standard is <1.0% for Mg/Ca.

5. Planktic Mg/Ca Results

[16] We present results from three species of planktic foraminifers in cores from five water depths ranging from 1.6 to 4.0 km (Figure 2). There were too few remaining *G. ruber* shells for analysis between 0 and 10 cm in the 3.4 km core (MW91-9 48GGC). There were enough *G. ruber* specimens in MW91-9 55GGC for a single trace metal sample, however, most of the samples dissolved during the cleaning process. In the cores that contain all three species, *G. ruber* generally has slightly higher Mg/Ca than *G. sacculifer* during both the Holocene and LGM. *N. dutertrei* has lower Mg/Ca than both *G. ruber* and *G. sacculifer* in all cores during both the Holocene and LGM.

[17] *G. ruber* and *G. sacculifer* have a similar glacial to interglacial Mg/Ca change (Figures 2a and 2b and Table 2). The Mg/Ca ratio of *G. ruber* and *G. sacculifer* are 18% and 14% lower respectively during the LGM than during the Holocene. In both species the glacial-interglacial decrease is slightly larger in the deeper cores than in the shallow cores. Consequently, the decrease in Mg/Ca with increasing water depth is slightly larger for both species during the LGM. During the Holocene the Mg/Ca ratio of *G. ruber* decreases 5% per km and the Mg/Ca ratio of *G. sacculifer* decreases 4% per km. During the glacial, there is a 6% decrease per km relative to the shallow core for *G. ruber* and 7% decrease per km relative to the shallow core for *G. sacculifer*. The decrease in the Mg/Ca ratio per km during the LGM in comparison to the Holocene is not statistically significant.

[18] The Mg/Ca results for *N. dutertrei* are in sharp contrast to the results of *G. ruber* and *G. sacculifer* (Figure 2c and Table 2). There is a large decrease in the Mg/Ca ratio with increasing water depth in comparison to both of the near surface dwelling species in both the Holocene and LGM. During the Holocene the Mg/Ca ratio decreases 14% per km. During the LGM the decrease is slightly larger, 18% per km. In addition, from the LGM into the deglaciation, the Mg/Ca ratio of *N. dutertrei* first increases to values in excess of the core top values and then decreases to modern values. The increase in the Mg/Ca ratio of *N. dutertrei* through the deglaciation is present in all cores.

6. Discussion

6.1. Separating the Effects of Temperature and Carbonate Ion Concentration

[19] The Mg/Ca variations through time recorded by the three species in these five cores reflect, to varying extents, differences in both temperature (temporally, i.e., down core) and preservation (with increasing water depth as well as down core). Lower temperatures and increased dissolution lead to lower Mg/Ca in all three species. Offsets in Mg/Ca values among the three species within a core initially arise from differences in the sensitivity of the Mg/Ca response of each species to temperature (i.e., species specific temperature–$D_{Mg/Ca}$ relationships). In addition, the differing Mg/Ca ratios among the species reflect differences in their depth habitats. The slightly lower Mg/Ca and heavier $\delta^{18}O$ for the *G. sacculifer* and substantially lower Mg/Ca and heavier

Table 2. Mg/Ca Data From Core Top, Holocene, Deglacial, and LGM Intervals

		N. dutertrei[a]			*G. ruber*[b]			*G. sacculifer*[c]		
Core ID	Depth (km)	Mg/Ca	ΔCO_3^{2-}	$[CO_3^{2-}]$	Mg/Ca	ΔCO_3^{2-}	$[CO_3^{2-}]$	Mg/Ca	ΔCO_3^{2-}	$[CO_3^{2-}]$
					Holocene					
MW91-9 6	1.6	2.10	25	83	4.37	25	83	3.85	25	83
MW91-9 34	2.0	2.00	20	83	4.13	9	72	4.03	36	99
MW91-9 38	2.5	1.74	7	76	4.14	9	78	3.94	31	100
MW91-9 48	3.4	1.43	−11	72	3.95	−4	79	3.57	7	90
MW91-9 55	4.0	1.35	−16	77				3.49		
					Deglacial					
MW91-9 6	1.6	2.24	33	91	4.30	-	-	4.01	-	-
MW91-9 34	2.0	2.27	34	97	4.19	-	-	3.97	-	-
MW91-9 38	2.5	1.93	19	88	4.03	-	-	3.74	-	-
MW91-9 48	3.4	1.67	6	88	3.86	-	-	3.69	-	-
MW91-9 55	4.0	1.50	−4	89						
					LGM					
MW91-9 6	1.6	2.13	38	95	3.60	-	-	3.32	-	-
MW91-9 34	2.0	1.92	28	91	3.28	-	-	3.21	-	-
MW91-9 38	2.5	1.40	−1	68	3.42	-	-	3.45	-	-
MW91-9 48	3.4	1.02	−30	53	3.24	-	-	2.89	-	-
MW91-9 55	4.0	1.12	−16	77						

[a]Decrease in Mg/Ca per kilometer for *N. dutertrei* is 14% for Holocene, 14% for deglacial, and 18% for LGM.
[b]Decrease in Mg/Ca per kilometer for *G. ruber* is 5% for Holocene, 6% for deglacial, and 6% for LGM.
[c]Decrease in Mg/Ca per kilometer for *G. sacculifer* is 4% for Holocene, 4% for deglacial, and 7% for LGM.

$\delta^{18}O$ for the *N. dutertrei* relative to *G. ruber* are consistent with their relative position in the water column (Figure 2). *G. ruber* and *G. sacculifer* are surface to subsurface dwelling spinose foraminifers that are thought to calcify in the mixed layer, and also have similar Mg-temperature sensitivities (see equations (1) and (2) below). *G. sacculifer* has a slightly deeper depth habitat (20–60 m) than *G. ruber* (0–30 m). *N. dutertrei* is a nonspinose thermocline species that occupies a depth range between 60–150 m [*Fairbanks and Wiebe*, 1980; *Fairbanks et al.*, 1982; *Farmer et al.*, 2007; *Spero et al.*, 2003]. *N. dutertrei* also has a lower Mg/Ca-temperature sensitivity than the other two species (see equation (3) below) [*Fehrenbacher et al.*, 2006; *Dekens et al.*, 2002].

[20] The initial Mg/Ca content, set by the calcification temperature, is modified by the different dissolution sensitivities of the shell Mg content of each species; this leads to varying glacial-interglacial Mg/Ca amplitudes among species within a single core as well as different Mg/Ca amplitudes among the species with increasing water depth (Figure 2). The most salient feature of the data with respect to interpreting past changes in deep-sea carbonate chemistry is the decrease in Mg/Ca with increasing water depth during any given time interval. That all three species show slightly larger decreases in Mg/Ca with increasing water depth during the glacial implies that there was a slightly steeper gradient in the saturation state of deep waters during the glacial relative to the modern (e.g., *N. dutertrei* shows a 14% change in Mg/Ca per km during the Holocene versus 18% during the glacial; Table 2). That is, there was slightly more intense dissolution in the deeper cores than in the shallow cores during the glacial relative to the Holocene. By the deglaciation, the change in the Mg/Ca ratio over the depth range of the suite of cores is comparable to the modern, implying a comparable ΔCO_3^{2-} gradient though not necessarily the same absolute values of ΔCO_3^{2}. That *N. dutertrei* has the largest decrease in Mg/Ca with depth over all time intervals is consistent with the larger response to changes in preservation for this species as has been shown in previous studies [*Dekens et al.*, 2002; *Fehrenbacher et al.*, 2006].

[21] To sort out the effects of depth habitat, temperature, and preservation on Mg/Ca and quantify the changes in deep water carbonate ion concentration for a given "time slice" we use the calibration equations based on core top data sets developed by *Dekens et al.* [2002] and modified by *Fehrenbacher et al.* [2006]:

$$G.\,ruber\text{: } \mathrm{Mg/Ca} = 0.37\exp[0.084(\mathrm{Temp}_{15m}) + 0.0034(\Delta CO_{3\,bw}^{2-})] \quad (1)$$

$$G.\,sacculifer\text{: } \mathrm{Mg/Ca} = 0.31\exp[0.084(\mathrm{Temp}_{30m}) + 0.0040(\Delta CO_{3\,bw}^{2-})] \quad (2)$$

$$N.\,dutertrei\text{: } \mathrm{Mg/Ca} = 0.50\exp[0.044(\mathrm{Temp}_{100m}) + 0.0109(\Delta CO_{3\,bw}^{2-})] \quad (3)$$

where the subscript on temperature denotes the average calcification depth of each species and the subscript "bw" on the ΔCO_3^{2-} denotes bottom water. The carbonate saturation state, ΔCO_3^{2-}, is defined as the difference between the in situ carbonate ion concentration ($[CO_3^{2-}]_{in\ situ}$) and the saturation carbonate ion concentration ($[CO_3^{2-}]_{sat}$) ($\Delta CO_3^{2-} = [CO_3^{2-}]_{in\ situ} - [CO_3^{2-}]_{sat}$).

[22] Using any one of these species-specific equations (1)–(3), we can quantitatively estimate the changes in ΔCO_3^{2-} between water depths using the decrease in Mg/Ca with increasing water depth (i.e., by quantitatively comparing the Mg/Ca from two cores). We use *N. dutertrei* for our glacial and deglacial reconstructions because of the larger effect of carbonate saturation state on *N. dutertrei* relative to the two surface dwelling species we analyzed and the smaller error

on the reconstructions as determined in our previous study [*Fehrenbacher et al.*, 2006]. First, we rewrite *N. dutertrei* equation (3) for the measured Mg/Ca at two depths:

$$\mathrm{Mg/Ca}_1 = 0.50\exp\left[0.044(\mathrm{Temp}_{100\mathrm{m}}) + 0.0109\left(\Delta\mathrm{CO}_3^{2-}\right)_1\right] \quad (4)$$

$$\mathrm{Mg/Ca}_2 = 0.50\exp\left[0.044(\mathrm{Temp}_{100\mathrm{m}}) + 0.0109\left(\Delta\mathrm{CO}_3^{2-}\right)_2\right] \quad (5)$$

where subscripts 1 and 2 denote the Mg/Ca and ΔCO_3^2 at contemporaneous intervals from two cores in the same region at different water depths (i.e., 1 could be the core at 1.6 km and 2 could be the core at 2.0 km). Second, we subtract equation (5) from equation (4), which eliminates temperature from the resulting equation. Rearranging the resulting equation yields equation (6), which relates a change in ΔCO_3^{2-} to the Mg/Ca from the two depths:

$$\left(\Delta\mathrm{CO}_3^{2-}\right)_1 - \left(\Delta\mathrm{CO}_3^{2-}\right)_2 = \frac{1}{0.0109}\ln\left(\frac{(Mg/Ca)_1}{(Mg/Ca)_2}\right) \quad (6)$$

where the left hand side of the equation is the finite change in ΔCO_3^{2-} between any two core depths:

$$\mathrm{d}\left(\Delta\mathrm{CO}_3^{2-}\right) = \left(\Delta\mathrm{CO}_3^{2-}\right)_1 - \left(\Delta\mathrm{CO}_3^{2-}\right)_2 \quad (7)$$

The above equations (6) and (7) can be used to estimate the ΔCO_3^{2-} gradient between cores for the Holocene, Deglaciation, and LGM. This allows for a direct comparison of the steepness of the ΔCO_3^{2-} gradient through time.

[23] To calculate the absolute ΔCO_3^{2-} at any given age and depth, from which we can then determine the $[CO_3^{2-}]_{\text{in situ}}$ concentration, we need additional information beyond the Mg/Ca of one species because there are two unknowns in the exact solution for the equation: temperature and ΔCO_3^{2-}. Here, we quantitatively estimate the ΔCO_3^{2-} at the depth of the shallow core by using constraints given by the measured Mg/Ca of a second species, *G. ruber*. By assuming a likely range of calcification temperatures for *N. dutertrei* relative to *G. ruber*, we can solve the *G. ruber* and *N. dutertrei* equations simultaneously (2 equations, 2 unknowns) and calculate a range of ΔCO_3^{2-} and thus the $[CO_3^{2-}]_{\text{in situ}}$ for different time intervals using:

$$G.\,ruber\text{: }(\mathrm{Mg/Ca})_{\mathrm{ruber,1.6km}} = 0.37\exp[0.084(\mathrm{Temp}_{15\mathrm{m}}) + 0.0034\left(\Delta\mathrm{CO}_3^{2-}\right)_{1.6\mathrm{km}}] \quad (8)$$

$$N.\,dutertrei\text{: }(\mathrm{Mg/Ca})_{\mathrm{duter,1.6km}} = 0.50 \cdot \exp[0.044(\mathrm{Temp}_{15\mathrm{m}} - \mathrm{T}_{\mathrm{offset}}) + 0.0109\left(\Delta\mathrm{CO}_3^{2-}\right)_{1.6\mathrm{km}}] \quad (9)$$

where the Mg/Ca of *G. ruber* and *N. dutertrei* are measured values from the shallowest core for any given time interval and T_{offset} equals a prescribed offset in temperature (see the following paragraph) between the surface dwelling species *G. ruber* and the thermocline species *N. dutertrei*. By prescribing the offset, we are left with two equations (8) and (9) and two unknowns ($Temp_{15m}$ and ΔCO_3^{2-}). Once the ΔCO_3^{2-} is calculated for the shallowest site, we can shift the previously calculated gradients to define absolute values of ΔCO_3^{2-} over the depth range of the cores. Alternatively, the ΔCO_3^{2-} could be calculated in any of the cores at any interval that contains both *G. ruber* and *N. dutertrei* (we term this the 'two-species approach'). Both approaches yield similar results and the error on the ΔCO_3^{2-} estimate is nearly identical (8 μmol/kg using the two species approach versus 9 μmol/kg using equation (6)).

[24] The absolute values of ΔCO_3^{2-} depend on the prescribed offset between the calcification temperatures for *G. ruber* and *N. dutertrei*, which can vary over time depending on the structure of the upper water column and species preferences. For the Holocene reconstruction we calculate the shallow core ΔCO_3^{2-} setting the T_{offset} equal to the modern temperature offset between the average calcification depth of *G. ruber* (20 m) and *N. dutertrei* (100 m), 1.9°C [*Farmer et al.*, 2007; *Levitus and Boyer*, 1994]. For the LGM and deglacial reconstruction we calculate a range of ΔCO_3^{2-} using three temperature offsets, which bracket the likely minimum and maximum ΔCO_3^{2-}. First, similar to the Holocene reconstruction, we use the modern temperature offset of 1.9°C. Second, we assume a likely maximum calcification temperature for *N. dutertrei* by assuming the surface dwelling *G. ruber* calcifies at a shallower depth than the deep dwelling *N. dutertrei*. *N. dutertrei* must have recorded a temperature that did not exceed the calcification temperature of *G. ruber* and we set the temperatures equal to each other. The second scenario is similar to assuming stratification was eliminated in the upper water column over the depth range of these species (0–150 m). While it is unlikely stratification was eliminated during any of the time periods this assumption constrains the maximum calcification temperature for *N. dutertrei* and the minimum ΔCO_3^{2-}. For every degree cooler the *N. dutertrei* calcification temperature the implied carbonate ion concentration is ~4.5 μmol/kg lower. Finally, we estimate a maximum calcification temperature offset between the two species based on the $\delta^{18}O$ difference between *G. ruber* and *N. dutertrei* (as discussed below for each reconstruction). The $\delta^{18}O$ difference implies a larger offset between the species and constrains our lower ΔCO_3^{2-} estimate. The approach could be improved by using two species that calcify at a similar water depth, eliminating the need for estimating a temperature offset; however, the equations for *G. ruber* and *G. sacculifer* are too similar to be linearly independent when error is considered (see equations (1) and (2) above and discussion of error by *Fehrenbacher et al.* [2006]). The combination of *G. ruber* and *N. dutertrei* is useful because of the stronger temperature and weaker carbonate ion effect on *G. ruber* relative to *N. dutertrei*.

6.2. Holocene ΔCO_3^{2-} Reconstructions

[25] We generate the shallow core ΔCO_3^{2-} based upon the two-species method described above using 1.9°C for the T_{offset}. We then use the change in the Mg/Ca ratio with depth (equation (5)) to generate the ΔCO_3^{2-} gradient relative to the shallow core. We use the same shallow core ΔCO_3^{2-} calculated using the T_{offset} between *G. ruber* and *N. dutertrei* for the *G. sacculifer* Holocene reconstruction, but note the shallow core ΔCO_3^{2-} results are nearly identical (2.8 μmol/kg lower) if we had opted to calculate the ΔCO_3^{2-} using the T_{offset} between *G. sacculifer* and *N. dutertrei*.

[26] The Holocene ΔCO_3^{2-} results reconstructed using *N. dutertrei* and *G. ruber* closely resemble the modern

gradient (Figures 3a and 3c). The *G. sacculifer* ΔCO_3^{2-} results are also similar to the modern gradient, but an average 10 μmol/kg higher than modern at all depths (Figure 3b). The good fit to the modern gradient using *N. dutertrei* is in agreement with our previous study which showed that the Holocene ΔCO_3^{2-} gradient reconstructed using the Mg/Ca ratios from *N. dutertrei* most accurately reproduced the modern Atlantic $[CO_3^{2-}]_{in\ situ}$ gradient [*Fehrenbacher et al.*, 2006].

[27] The error on the ΔCO_3^{2-} reconstruction is small for *N. dutertrei*, ~9 μmol/kg, and much larger for *G. ruber* and *G. sacculifer*, ~28 μmol/kg [*Fehrenbacher et al.*, 2006]. The smaller error on the *N. dutertrei* reconstruction is likely due to the stronger response this species has to changes in carbonate chemistry in comparison to *G. ruber* and *G. sacculifer* [see *Fehrenbacher et al.*, 2006, Figure 8]. The greater sensitivity of the *N. dutertrei* Mg/Ca to changes in dissolution together with the good fit to the modern gradient, the smaller error on the reconstruction, and the results of our Atlantic study suggests that *N. dutertrei* best records changes in preservation. In the following sections, we focus on the *N. dutertrei* Mg/Ca results to reconstruct LGM and deglacial carbonate ion gradient.

6.3. Last Glacial Maximum Carbonate Ion Reconstruction

[28] For the LGM we calculate a range of ΔCO_3^{2-} using prescribed temperature offsets: 1.9°C, 0.0°C, and the maximum temperature offset implied by the $\delta^{18}O$ difference between the *G. ruber* and *N. dutertrei*. The oxygen isotope difference between *G. ruber* and *N. dutertrei* during the LGM is ~0.5‰ larger than modern (core top). By assuming a 0.23‰ change in $\delta^{18}O$ per °C we obtain an additional temperature offset of 2.2°C larger than modern; thus the third temperature offset is 4.1°C (the modern offset of 1.9°C plus 2.2°C).

[29] The results suggest the LGM ΔCO_3^{2-} is similar to or higher than modern in the shallow two cores and drops below modern between 2.0 and 2.5 km. Below 2.5 km, the ΔCO_3^{2-} is at a minimum an average ~7 μmol/kg lower than modern and at a maximum an average ~27 μmol/kg lower than modern (Figure 4a). The maximum temperature offset (4.1°C) yields very high ΔCO_3^{2-} at the depth of the shallow core, high enough to preserve pteropods. There were no pteropods in the glacial intervals and therefore find the maximum T_{offset}, that yields the highest ΔCO_3^{2-}, unlikely, at least for the glacial. The $\delta^{18}O$ difference between *G. ruber* and *N. dutertrei* is larger during the LGM, suggesting a larger temperature difference between the two species during the LGM in comparison to the modern. Thus, we find the likely calcification temperature offset between *G. ruber* and *N. dutertrei* to be greater than 1.9°C and smaller than 4.1°C. The gray bar in Figure 4a denotes the corresponding likely ΔCO_3^{2-} for this region during the LGM.

6.4. Deglacial Carbonate Ion Gradient and in Situ Concentrations

[30] Similar to the approach for the LGM reconstruction above, we bracket the ΔCO_3^{2-} using assumptions about the offset in temperature between *G. ruber* and *N. dutertrei*: 1.9°C, 0.0°C, and the temperature offset implied by the deglacial oxygen isotopic offset between *G. ruber* and *N. dutertrei* during the deglacial (0.6‰ larger than the modern offset or an additional 2.6°C). In all cases, the ΔCO_3^{2-} implies better carbonate preservation at all depths (with the exception of the deepest core in the no temperature offset case) in comparison to modern (Figure 4b).

[31] While the >4°C temperature offset between the surface dwelling *G. ruber* and the thermocline dwelling *N. dutertrei* may seem large relative to the modern offset in this region, larger temperature differences between these two species are observed in the modern ocean in other regions. For example, in the eastern equatorial Pacific the temperature offset between these two species, implied by their Mg/Ca ratios, can exceed 10°C, consistent with the stratification of the upper water column in this region. In addition, the $[CO_3^{2-}]_{in\ situ}$ implied by the ~4.5°C temperature offset is consistent with the presence of pteropods in the shallowest two cores. At 2.0 km, the depth of the deepest core that contained an abundance of pteropods, the $[CO_3^{2-}]_{sat}$ for aragonite is 103 μmol/kg, ~38 μmol/kg higher than the $[CO_3^{2-}]_{sat}$ for calcite [*Zeebe and Wolf-Gladrow*, 2001]. Using the 4.5°C temperature offset, the calculated $[CO_3^{2-}]_{in\ situ}$ at 2.0 km is ~109 μmol/kg, high enough to preserve pteropods. This lends confidence that the large temperature offset between *G. ruber* and *N. dutertrei* is the most likely for the deglaciation and the maximum carbonate ion concentration inferred from the reconstruction is the most probable (denoted by the gray arrow in Figure 4b). We note any bioturbation in these cores would have attenuated the deglacial spike by mixing lower Mg/Ca *N. dutertrei* from LGM and Holocene intervals, thus rendering our deglacial reconstruction a minimum estimate. See section 6.6 for an assessment of bioturbation on the carbonate ion reconstructions.

6.5. Paleoceanographic Implications for the Glacial and Deglacial Pacific

6.5.1. Paleoceanographic Implications for the Glacial Pacific

[32] The carbonate ion concentration reconstructions at the depth of the shallow two cores is similar to or higher than modern, consistent with the view of similar to slightly better preservation during the LGM; at least above 2.5 km. Taken at face value, between 2.5 and 4.0 km the ΔCO_3^{2-} is an average 7–27 μmol/kg lower over the depth range), implying more undersaturated waters in the deep Pacific during the LGM and a ~1 km or more shoaling of the lysocline relative to the modern (Figure 4a). While this is in sharp contrast to the long held picture of better preservation in the glacial Pacific suggested by *Farrell and Prell* [1989], it is consistent with the reconstruction for the Ontong Java Plateau by *Wu et al.* [1991] that used percent carbonate content to infer a 1 km shallower lysocline. It is also somewhat consistent with findings of *Broecker and Clark*'s [2003] glacial ΔCO_3^{2-} reconstruction based on foraminiferal shell weight that implies more intense dissolution during the LGM (between 2.3 and 4.0 km) and the slightly lower glacial carbonate ion concentration in the eastern equatorial Pacific implied by the Zn-CO_3^{2-} proxy [*Marchitto et al.*, 2005].

[33] *Farrell and Prell*'s [1989] oft-cited reconstruction of deep Pacific preservation cycles over the last 650 kyr, based on percent calcite in sediments from the deep equatorial Pacific, suggests glacial periods are marked by a deeper

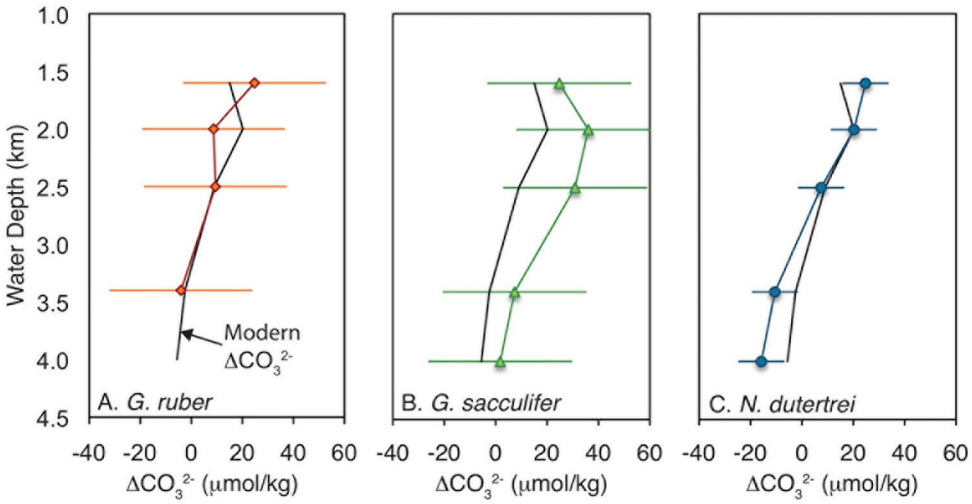

Figure 3. Modern (black line) and reconstructed Holocene ΔCO_3^{2-} gradient versus core depth reconstructed using the Mg/Ca ratio from three planktic species. The modern ΔCO_3^{2-} gradient was reconstructed using GEOSECS data as reported by *Dekens et al.* [2002]. The (a) *G. ruber* (orange diamonds) and (c) *N. dutertrei* (blue circles) ΔCO_3^{2-} reconstructions most closely reflect the modern gradient. The ΔCO_3^{2-} gradient reconstructed from (b) *G. sacculifer* (green triangles) yields values similar to modern in the shallow and deep cores and higher than modern values in the middepth cores. The error bars represent the error in carbonate ion concentration reconstructed from the calibration data set [*Fehrenbacher et al.*, 2006].

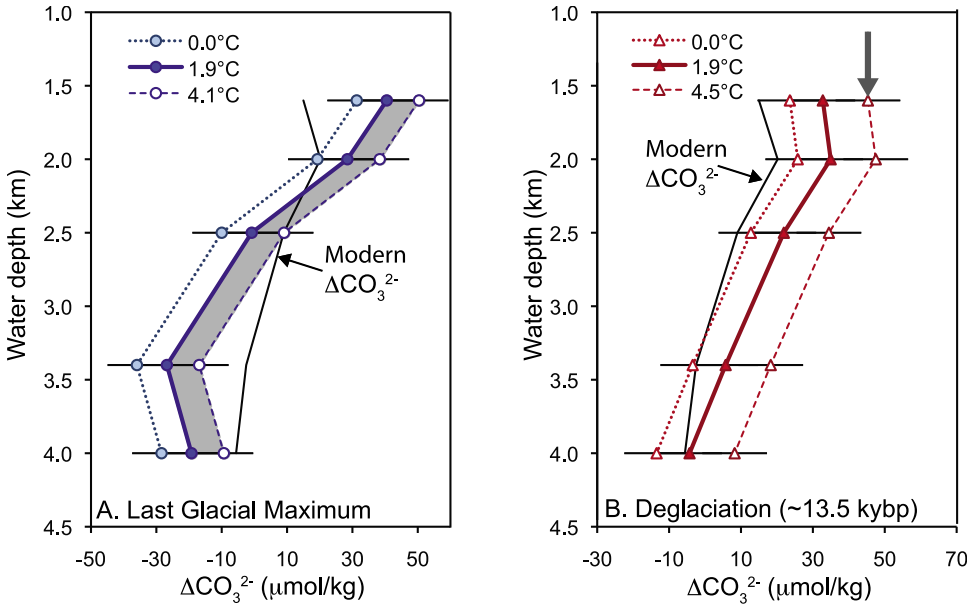

Figure 4. The ΔCO_3^{2-} reconstructions for the (a) LGM and (b) deglaciation. For both reconstructions the ΔCO_3^{2-} at the depth of the shallow core was estimated using the two species approached outlined in the text. The ΔCO_3^{2-} profiles are based on the decrease in the Mg/Ca ratio of *N. dutertrei* with increased water depth. In both plots, the left-most line is the ΔCO_3^{2-} reconstruction under the assumption of no temperature stratification of the upper water column (i.e., no calcification temperature offset between *G. ruber* and *N. dutertrei*). The middle line is the reconstruction using the modern temperature offset between *G. ruber* and *N. dutertrei* (1.9°C). The right-most line is the ΔCO_3^{2-}gradient under the assumption of enhanced temperature stratification based on the oxygen isotopes of *G. ruber* and *N. dutertrei*. See text for details.

lysocline and enhanced calcite preservation whereas interglacials are marked by a more shallowly inclined, deeper lysocline and a decrease in calcite preservation. Their low-resolution study focused on the long 100 kyr preservation cycles in the deepest pacific (4.2 to 5.0 km) in contrast to our study which is higher resolution, at shallower depths, and focuses on only the last 25 kyr.

[34] We note several possible complications of their study. First, the resolution of their reconstruction is low; thus, resolving for changes within a full glacial cycle is difficult. Second, it is possible that the results of their study are recording changes in productivity rather than changes in dissolution [*Archer*, 1991]. Third, several of their deeper cores were located away from the equator and had lower sedimentation rates than the cores located on the equator, which could bias their reconstruction. Finally, we also note a possible complication in interpreting changes in preservation using percent carbonate content of sediments. Culturing studies have shown that foraminiferal shell weight and shell thickness increase as a function of surface $[CO_3^{2-}]$ [*Bijma et al.*, 2002; *Billups and Schrag*, 2002]. During the LGM, the $[CO_3^{2-}]$ of surface waters would have been higher than modern due to the lower pCO_2 of the atmosphere. It is possible that the thicker shelled foraminifera produced during glacial periods (as noted by *Barker and Elderfield* [2002]) could have been more resistant to whole shell dissolution than interglacial foraminifera (which would have thinner walls) thus complicating their reconstruction even further. Although, this might also affect *Wu et al.*'s [1991] interpretation based on shell fragmentation index.

[35] The shape of the gradient and the carbonate ion concentration at the different depths can be explained as a combination of changes in circulation and deep ocean carbonate chemistry in the Pacific during the LGM. In the modern Pacific Ocean, deep flow is dominated by dense Circumpolar Deep Water (CDW) that enters the Pacific basin from the Southern Ocean. This water mass flows north where it is upwelled and then returns south as Pacific Deep Water (PDW), generally below 1.5 km. The result is relatively constant $[CO_3^{2-}]_{in\ situ}$ with depth and a modern ΔCO_3^{2-} gradient in the deep Pacific that is controlled primarily by the pressure effect on saturation. Our results for the LGM show an overall steeper gradient and a sharp contrast in carbonate chemistry that lies between 2.0 and 2.5 km suggesting the presence of more than one water mass in this region of the deep Pacific. The significantly more undersaturated waters bathing the deep sites (>2.5 km) suggest a change in the carbonate chemistry of the source waters.

[36] A reconstruction of glacial Pacific circulation suggests that deep-water circulation during the LGM differed greatly from the general circulation in the modern Pacific Ocean [*Matsumoto et al.*, 2002]. The LGM circulation reconstructed based on the $\delta^{13}C$ of benthic foraminifera, a quasi-conservative water mass tracer, suggests a more sluggish CDW entered the Pacific basin and returned south as PDW at greater depths, generally deeper than 2 km [*Herguera et al.*, 1992; *Keigwin*, 1998; *Matsumoto et al.*, 2002]. Studies have suggested that the water mass that dominated the Southern Ocean (SOW), the source water for PDW, were the saltiest waters of the glacial ocean [*Adkins et al.*, 2002] and had ventilation ages that are 500 years older than modern [*Shackleton et al.*, 1988]. The older, more dense water mass may have accumulated more carbon than the modern SOW and would therefore have a higher pCO_2/lower $[CO_3^{2-}]_{in\ situ}$. This water mass would have fed the deep Pacific during the LGM and, if the reconstruction of *Matsumoto et al.* [2002] accurately depicts the glacial circulation pattern, would not have extended to depths shallower than 2.5 km. Our ~23 μmol/kg decrease in carbonate ion concentration, suggested by our Mg/Ca data, is consistent with the presence a water mass boundary below ~2.5 km.

[37] The general circulation pattern above 2 km is not agreed upon. The flow could have been a south flowing NPIW that formed at greater depths, a north flowing Glacial North Atlantic Intermediate Water (GNAIW), or a combination of the two [*Matsumoto et al.*, 2002]. Benthic geochemical data are sparse in the shallower water depths of the Pacific basin, which makes a definitive assessment of the water mass distribution shallower than 2 km difficult to determine. Our reconstruction does not provide enough information to determine which water mass (NPIW or GNAIW) was present shallower than 2 km in the western equatorial region during the LGM; but, our reconstruction confirms the presence of an upper (<2.5 km) water mass that has higher carbonate ion concentration, i.e., is more recently ventilated and/or is more nutrient depleted, than the water mass below 2.5 km.

6.5.2. Paleoceanographic Implications for the Deglacial Pacific

[38] The shape of the carbonate ion gradient during the deglaciation is similar to the modern gradient suggesting the circulation during the deglaciation was similar to modern circulation or at least that the cores are all bathed in the same water mass (below 1.6 km) as we observe today. The presence of pteropods in the shallow three cores (1.6 to 2.5 km) suggests the maximum carbonate ion gradient estimated by our reconstruction is likely the most accurate. Globally, the aragonite compensation depth (ACD) is on average 1 km shallower than the calcite compensation depth (CCD) in the modern ocean [*Sarmiento and Gruber*, 2006]. In the modern Pacific, pteropods are ubiquitous in the surface waters [*Lalli and Gilmer*, 1989; *van der Spoel and Heyman*, 1983]. However, deposition of pteropods does not occur deeper than 1.5 km depth, even shallower on the Ontong Java Plateau (0.5–1.0 km), the region where our samples were obtained [*Berger*, 1978]. Many studies suggest the depth of the ACD deepened during the deglaciation, which resulted in a deglacial pteropod preservation 'spike' that is noted in several locations globally [*Berger*, 1977, 1978; *Ganssen et al.*, 1991; *Melkert et al.*, 1992; *Shackleton and Opdyke*, 1977; this study]. The results presented herein show that the preservation was enhanced for foraminifers as well during this time period. The Mg/Ca ratio increases in all three planktic species used in this study, though it is most pronounced in *N. dutertrei* whose deglacial Mg/Ca value exceeds its modern Mg/Ca values.

[39] There are several mechanisms that could have triggered higher carbonate ion concentration and the deepening of both the ACD and CCD during the deglaciation. Following ice sheet retreat an increase in terrestrial biomass would have sequestered a large amount of CO_2, which would result in an increase in the carbonate ion concentration of the deep ocean. However, the deglacial biomass

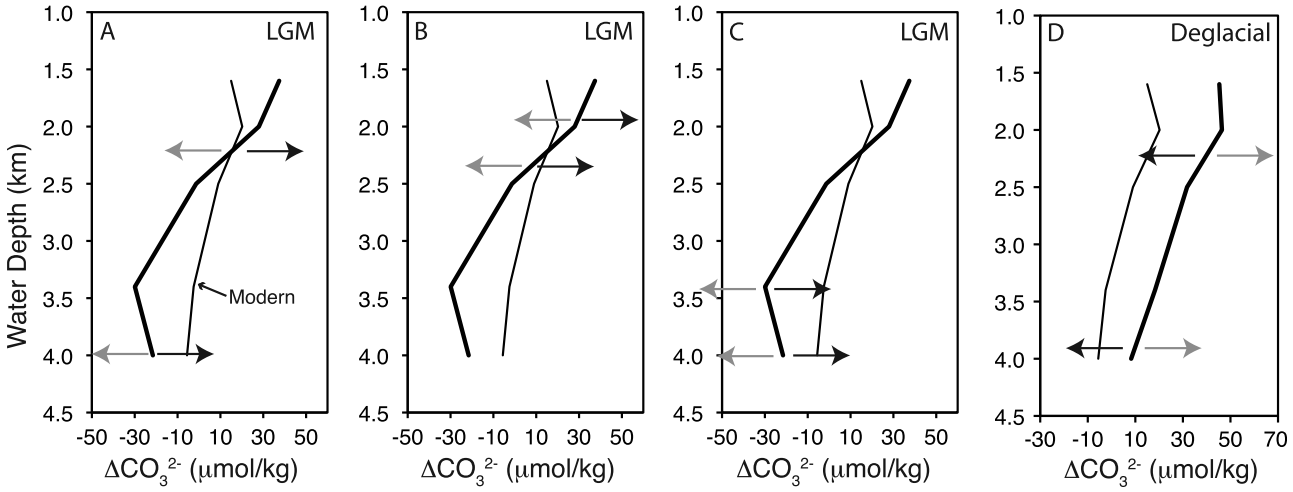

Figure 5. A schematic illustration of the effect of bioturbation on the carbonate ion reconstructions presented in this study. (a) If bioturbation is the same at all depths and higher Mg/Ca ratio foraminifera mix into the LGM interval, the reconstruction is shifted in the direction of better preservation (black arrows). Mixing would make the carbonate ion concentration reconstructed appear higher than it actually was and the actual carbonate ion concentration would be lower (gray arrows). (b) More intense bioturbation in the shallow cores would preferentially shift the shallow core reconstructions in the direction of better preservation, resulting in a steeper gradient with depth and the appearance of better preservation in the shallow cores (black arrows). The actual carbonate ion concentration would then be lower and the true gradient with depth in this scenario would be less steep (gray arrows). (c) Though unlikely, if mixing intensity were more intense in the deeper cores, the carbonate ion concentration of the deeper cores would be shifted toward better preservation (black arrows). The "true" carbonate ion concentrations in this scenario would be lower in the deeper cores, suggesting a steeper gradient existed during the LGM. (d) Mixing of Holocene or LGM *N. dutertrei* into the deglacial intervals would lower the high Mg/Ca ratios of the deglacial (black arrows). Suggesting the reconstruction on the basis of the actual data represents a minimum change in the carbonate ion concentration.

increase did not occur until the Holocene. The deglacial rise in sea level could be a potential driver of an increase in the carbonate ion concentration as carbon storage on newly submerged shelves increased, however, similar to the increase in biomass, the post LGM rise in sea level occurred gradually through the deglaciation increasing by only about 30% by the time of our deglacial preservation spike and with an even smaller percentage of the full glacial – interglacial change in shelf area [*Clark et al.*, 2004; *Lambeck and Chappell*, 2001; *Montenegro et al.*, 2006]. Both the increase in terrestrial biomass and rise in sea level occurred too late in the deglaciation to be plausible mechanisms for the deglacial preservation peak.

[40] The higher carbonate ion concentration suggests a change in the chemical composition of the source waters. One possible mechanism consistent with results of recent studies could be a transfer of deep ocean CO_2 to the surface ocean and eventually the atmosphere, which would cause an increase in the deep ocean carbonate ion concentration and transient increase in calcite burial. The enhanced burial would have been driven by the resulting increase in $[CO_3^{2-}]_{in\ situ}$ of the deep ocean and the process of carbonate compensation. This process, which operates a time scale of 5–10 kyr, would have driven an increase in carbonate preservation in sediments until equilibrium is reached. The average 23 μmol/kg increase in $[CO_3^{2-}]_{in\ situ}$ suggested by the deglacial reconstruction implies that the burial rate of calcium carbonate during the deglaciation was approximately 1.5 times greater than the present burial rate [*Archer et al.*, 2000]. As recorded in Antarctic ice cores, atmospheric pCO_2 began to increase around 18 ka with an abrupt increase in pCO_2 around 14 ka [*Monnin et al.*, 2001]. Recent research supports a deep ocean source for the rise in atmospheric CO_2 based upon deglacial radiocarbon activity ($\Delta^{14}C$) reconstructions [*Galbraith et al.*, 2007; *Marchitto et al.*, 2007]. These studies imply a deep ocean carbon reservoir exhaled into the atmosphere, with both the Southern Ocean and North Pacific as viable locations for a transfer of CO_2 from the deep ocean to the atmosphere.

6.6. Caveats: Assessing Sediment Mixing and Error in the Age Models

6.6.1. Sediment Mixing

[41] Bioturbation by benthic organisms can attenuate the signals recorded by planktic foraminifera [*Anderson*, 2001]. The apparent timing of peak events can also be shifted, generally to older ages. The extent of attenuation as well as apparent shifts in the peak of any event may depend upon the sedimentation rate and the amount of organic matter available for the bioturbating organisms. Bioturbation is likely not uniform from within a suite of cores spanning a depth range, such as this study where depths span 1.6–4.0 km. Shallow cores may have higher bioturbation rates and/or deeper mixing zones owing to the higher organic

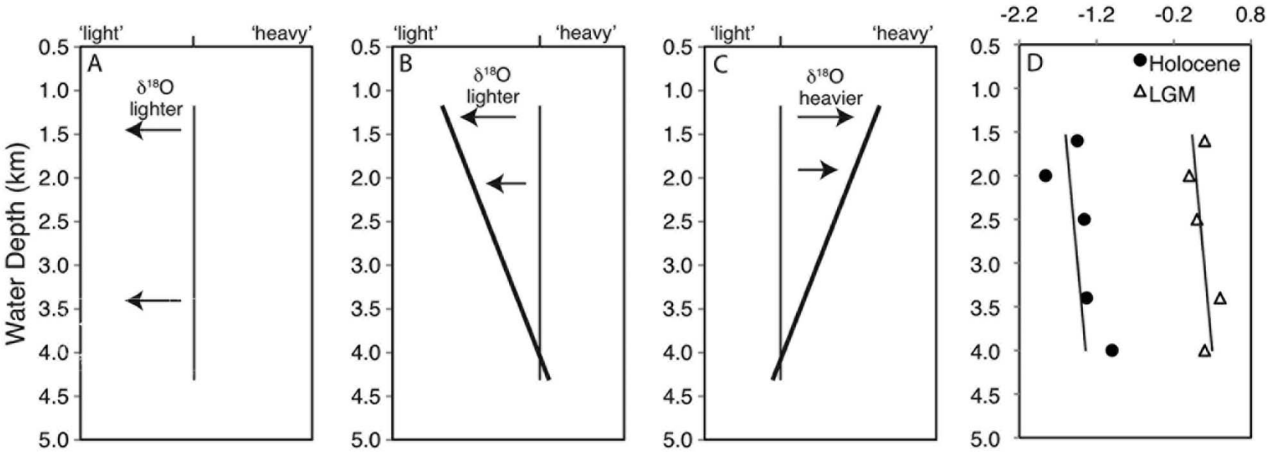

Figure 6. A schematic illustration of the effect of bioturbation on the oxygen isotopes. (a) If bioturbation is the same at all depths and heavier Holocene/deglacial foraminifers are mixed into the deglacial, the $\delta^{18}O$ values are shifted uniformly to heavier values. (b) If bioturbation were more intense in the shallower cores the shallow cores would have heavier $\delta^{18}O$ isotope values due to more Holocene/deglacial foraminifers resulting in a smaller $\Delta\delta^{18}O$ amplitude in the shallower cores. (c) If bioturbation were more intense in the deep cores the deep core $\delta^{18}O$ values would be heavier than the shallow cores resulting in smaller $\Delta\delta^{18}O$ amplitudes in the deeper cores. (d) Holocene and LGM $\delta^{18}O$ data. The Holocene and LGM $\Delta\delta^{18}O$ values are similar with depth (with the exception of the deepest core during the Holocene) suggesting bioturbation was similar at all depths during both the Holocene and LGM.

matter content at shallow depths. The thickness of the mixing zone in deep sea cores is thought to be approximately 8 cm [*Peng and Broecker*, 1984].

[42] The two most significant features of our reconstructions are (1) similar or slightly lower carbonate ion below 2.5 km in the Pacific during the last glacial maximum and (2) the deglacial peak in carbonate ion concentration. The cores used in this study have low sedimentation rates (1–2 cm/kyr) and, given the low sedimentation rate relative to the assumed thickness of the mixing zone, bioturbation may have attenuated the changes in the carbonate ion concentration implied by our time slice reconstructions. That is, mixing could have reduced the amplitude of the features we identify; thus, our estimates are likely to be a minimum change in the carbonate ion concentration. As we discuss in the following paragraphs, the combination of $\delta^{18}O$ and Mg/Ca data, and, for the deglacial events, the added constraints provided by the presence of pteropods, provide evidence that our most significant features are unlikely to be attributed to bioturbation.

[43] Our conclusion that the carbonate ion concentration was either similar to or lower than modern at depths deeper than 2.5 km during the LGM is based on comparison of the relative amplitude of the Mg/Ca changes in shallower cores versus deeper cores. Mixing scenarios and $\delta^{18}O$ help to sort the effects of bioturbation on the LGM intervals. Mixing intensity could have been (1) equal among all of the cores, (2) relatively stronger in the shallower cores, or (3) relatively stronger in the deeper cores. If mixing intensity were similar at all core depths during the LGM and deglacial foraminifers mixed into the LGM, the LGM Mg/Ca ratios would nearly uniformly shift from low LGM Mg/Ca ratios to higher deglacial ratios, shifting the reconstructed carbonate ion results in the direction of better preservation than the actual carbonate ion concentration. In this scenario, $\delta^{18}O$ of the planktic foraminifers would be nearly uniform among depths (Figure 5a). Alternatively, bioturbation could have been more intense in the shallow cores (such as might occur with greater organic content in these cores). More intense mixing in the shallow core(s) would likely mix more deglacial foraminifers with higher Mg/Ca and lighter $\delta^{18}O$ (relative to the deep cores) into the LGM intervals. The unequal mixing would lead to a shift that would look like better preservation in the shallow core relative to the modern and would yield a steeper reconstructed gradient for the LGM (Figure 5b). In this case, the $\delta^{18}O$ of the shallow cores would be lighter than the deep cores (Figure 6b). A third "end-member" scenario is that the deeper cores mixed more intensely than the shallow cores. More intense mixing in the deeper cores would increase Mg/Ca ratios in the LGM intervals of the deeper cores and preservation would then appear enhanced in the deep cores in comparison to the shallow cores (Figure 5c). In this case, the $\delta^{18}O$ of the deep cores would be lighter than the shallow cores (Figure 6c).

[44] The modern and LGM $\delta^{18}O$ gradients are similar among this suite of cores. The amplitude of the glacial to interglacial $\delta^{18}O$ is smaller than in some higher resolution cores and implies that the amplitude of our reconstructed carbonate ion concentrations has likely been attenuated (Figure 6d). However, the shallow slope of the $\delta^{18}O$ suggests mixing intensity was similar at all depths. If the entire suite of LGM values is considered, there is a slight trend toward heavier $\delta^{18}O$ values in the deeper cores implying slightly less mixing of deglacial or interglacial values in these intervals. The direction of this bias may be consistent with making the gradient appear slightly higher (toward lower carbonate ion in the deep cores); however, the difference in the $\delta^{18}O$ among the cores is very small suggesting

this is a minimal bias. Furthermore, it is worth noting that we reach a similar conclusion about the carbonate ion content of the deep waters during the LGM by simultaneously solving for temperature and carbonate saturation state using only the Mg/Ca of *N. dutertrei* and *G. ruber* in any of the cores below 2.5 km. That our results are similar whether we compare the gradient among the cores or whether we use data from any given core suggests that it is unlikely that our conclusion is an artifact of differential mixing of the two species of planktic foraminifers or differential mixing among the cores. Nonetheless, the potential effects of bioturbation should be kept in mind when comparing reconstructions at this site with other locations.

[45] For the deglacial carbonate ion peak we identify, the presence of (aragonitic) pteropods during the deglacial (~14 ka) coincident with increased Mg/Ca ratio of *N. dutertrei*, a species whose Mg/Ca ratio strongly responds to changes in the calcite saturation state and only weakly responds to temperature, supports our interpretation that the Mg/Ca increase was driven by carbonate saturation state at depth. Pteropods are present in the deglacial in the three shallowest cores, but are not present during the Holocene or glacial sections. Quantitatively, our reconstructed peak in carbonate ion concentration during the deglacial relies primarily on the strong dissolution and weak temperature response of *N. dutertrei* and is further constrained by the Mg-derived temperatures of coincident *G. ruber*. Based on core top calibration equations, the temperature needed to explain the Mg/Ca ratio of the deglacial peak for *N. dutertrei* is 32.5°C during the peak of this event, nearly 5°C higher than modern thermocline temperatures and 4°C higher than *G. ruber* during the deglaciation if changes in carbonate ion concentration are neglected (i.e., presumed to be the same as modern). Given *G. ruber*'s weaker response to carbonate ion, the Mg/Ca derived temperature for *G. ruber* using modern carbonate ion concentration is 28.5°C. While the oxygen isotopes for *G. ruber* and *N. dutertrei* suggest stratification was enhanced during this time period in comparison to modern (comparison of Figures 2d and 2f), the Mg/Ca derived temperature for *N. dutertrei* should not have exceeded that of *N. dutertrei* even if stratification were eliminated given the deeper calcification depth of *N. dutertrei*. Mixing of Holocene or LGM *N. dutertrei* shells into the deglacial intervals, would lower the deglacial *N. dutertrei* Mg/Ca ratio, rendering the deglacial results a minimal value (Figure 5d).

[46] We note an additional caveat associated with the suite of cores used in this study: sediment focusing and winnowing, a process by which sediment is preferentially removed from topographic highs and cores located a few degrees above and below the equator and deposited at greater depths and directly along the equator. *Wu et al.* [1991] suggested sediment focusing and winnowing as a likely cause of attenuated paleoceanographic signals in cores several degrees above and below the equator due to sediment winnowing while enhanced paleoceanographic signals results in cores along the equator due to the focusing of sediment. The shallowest core used in this study is located 2°S of the equator and the other cores are directly on the equator. Thus, the core located off of the equator and those shallower than 2.5 km may have experienced the winnowing of sediment while the others have perhaps gained sediment through focusing. It is difficult to ascertain the direct affects of this process given that our cores have also likely experienced differential dissolution (discussed above) and thus sorting the effects of both are difficult. However, if some sediment has been removed from the shallower cores and deposited along the deeper cores, dissolution could be enhanced in the deeper cores and attenuated in the shallower cores due to the transport of additional organic matter from the shallower cores. We note that biogenic, authigenic, and detrital sediments are affected to a similar degree by the processes of focusing and winnowing [*Higgins et al.*, 1999], thus, we expect any enhanced sedimentation and the effect on dissolution should be minimal.

6.6.2. Age Model Error

[47] Studies have shown that species offsets in low sedimentation rate cores can exceed 2000 years. Our age models are based on *G. sacculifer* radiocarbon ages coupled with $\delta^{18}O$ analyses. The $\delta^{18}O$ data for *N. dutertrei* and the *G. sacculifer* radiocarbon age models are in general agreement with the depth of the LGM in each of the cores, suggesting any error in our age models is minimal. Additionally, for the LGM and deglaciation we average three intervals together to obtain an average Mg/Ca measurement used in our reconstructions. The intervals span 1600 to 2000 years, thus, any error in the age model is likely captured by the time averaged data used for the reconstructions. However, in order to assess the robustness of our results we shift the age of the LGM by ~2000 years older and younger obtain new reconstructions based on the different Mg/Ca data (Figure 7). If the depth of the LGM is actually 2000 years older than our age model suggests, the results are nearly identical to the original results (Figure 7, dashed line, triangle symbols). If the age model is in error and the depth of the LGM is 2 kyr younger then the boundary between the two water masses suggested by our original results shifts to a deeper depth, between 2.5 and 3.4 km rather than between 2.0 and 2.5 km (Figure 7, dotted line, diamond symbols). The original results, however, that the deepest cores are bathed in a more corrosive water mass with lower carbonate ion concentration and the shallower cores are bathed in a more ventilated water mass with higher carbonate ion concentration remains unchanged.

7. Synthesis and Conclusions

[48] In our previous study we showed that a suite of cores could be used to estimate the relative carbonate ion gradient (that is, the change in carbonate ion concentration with depth) using the shallow core to calculate temperature and the change in the Mg/Ca ratio with depth to calculate the carbonate ion gradient. In this study, we apply a similar approach but here estimate a likely range of the carbonate ion concentration using two species-specific calibration equations and solving simultaneously for carbonate ion concentration (and temperature) in the shallow core. This method improves estimates of carbonate saturation state in the entire suite of cores and allows us to address more fully glacial-interglacial changes in deep-water carbonate chemistry. This alternative approach could be used to determine carbonate ion concentration in any single core, thereby eliminating the need for a suite of cores. We note that age offsets between different species in the same horizon could limit this new approach if the calcification temperature changed greatly over the period of time spanned by the age offset.

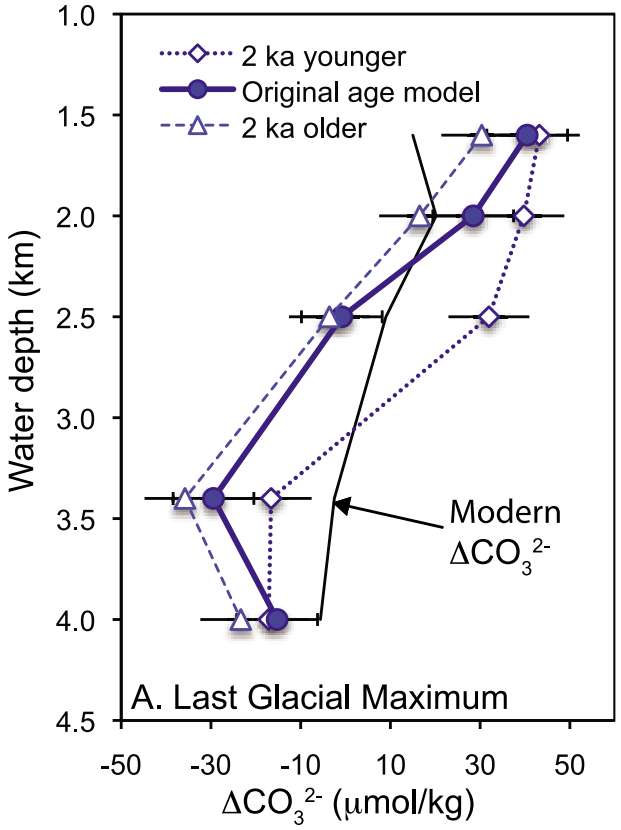

Figure 7. Assessment of error based on the age models for each core. We move the age of the LGM 2000 years older and 2000 years younger to assess the robustness of our results given any error in our age model construction. We find that any error smaller than ±2000 years has little effect on the overall results with the exception of a possible difference in the depth of the water mass shift present during the LGM if the actual LGM depth were 2000 years younger. We do not repeat this assessment for the deglaciation as the presence of pteropods and increase in Mg/Ca in *N. dutertrei* suggests the age of this interval to be well constrained.

[49] Our Mg-derived reconstruction of the ΔCO_3^{2-} for the LGM shows the shallow waters (above 2.0 km) may have had slightly higher ΔCO_3^{2-} than modern, but that the deepest waters in the Pacific had a lower saturation state than the modern corrosive waters of the deep Pacific. It appears the deep Pacific carbonate chemistry is more complex than a simple shift in the depth of the lysocline. Our results, along with other Pacific dissolution reconstructions based on a variety of proxies, suggest that the long-held view of better preservation during the LGM in the entire deep Pacific be reevaluated [*Broecker and Clark*, 2003; *Marchitto et al.*, 2005; *Wu et al.*, 1991].

[50] The carbonate ion gradients reconstructed here offer a view of the evolution of water mass circulation and carbonate chemistry over the last ~25,000 years in the western equatorial Pacific. Overall, the steeper $[CO_3^{2-}]$ gradient during the LGM with a distinct boundary between 2.0 and 2.5 km implies the presence of two deep Pacific water masses between 1.6 and 4.0 km. This is consistent with circulation changes implied by $\delta^{13}C$ [see *Matsumoto et al.*, 2002, and references therein] and radiocarbon from previous studies; however, the radiocarbon reconstruction by *Broecker et al.* [2007] places the boundary slightly deeper. Although we cannot pinpoint the source of the intermediate water mass (i.e., northern (NPIW) or southern (AAIW) source), we note that the carbonate chemistry suggests at most a water mass only slightly more nutrient depleted and well ventilated than modern waters in this region. With additional data from other regions in the Pacific, these geochemical constraints could help to identify the source waters for the upper water mass. Whatever the source of the shallower water mass, our results are consistent with the deepening of Pacific overturning circulation.

[51] During the deglacial interval, ~14 ka, the $[CO_3^{2-}]_{in\ situ}$ is higher by an average 23 μmol/kg than modern over the entire depth range, implying better preservation at all depths (between 1.6–4.0 km). The presence of pteropods suggests this value is likely representative of the ΔCO_3^{2-} during this time and the lower ΔCO_3^{2-} estimates based on the lower $T_{offsets}$ between *N. dutertrei* and *G. ruber* are not likely. We attribute a higher deglacial carbonate ion concentration to either a change in end-member carbonate chemistry or, possibly, a whole ocean shift in carbonate chemistry, as evidence from other localities suggests the preservation event was global [*Berger*, 1977, 1978; *Ganssen et al.*, 1991; *Melkert et al.*, 1992]. The relative uniformity in the $[CO_3^{2-}]_{in\ situ}$ (converting the ΔCO_3^{2-} to $[CO_3^{2-}]_{in\ situ}$) over the depth range during the deglacial implies that there was only one water mass occupying the deep tropical Pacific below 1.6 km, thus by the deglacial the deep Pacific appears to have established a circulation pattern similar to modern.

[52] The *G. ruber* Mg-derived SST suggests a glacial cooling of ~3°C and deglacial temperatures less than 1°C cooler than modern. Our temperature reconstruction is similar to other reconstructions from this region; temporal changes in carbonate ion concentrations have a small effect (<0.5°C) on the reconstructed temperatures for *G. ruber* in the shallowest core with a slightly larger effect in the deepest cores. Ignoring any changes in carbonate ion concentration, the Mg-derived temperatures of the deep dwelling foraminifera *N. dutertrei* suggest an elimination of stratification during the LGM. During the preservation event during the deglaciation, when *N. dutertrei* values are quite high, the deglacial Mg/Ca-derived temperature derived for *N. dutertrei* (32°C) is higher than *G. ruber* and exceeds modern thermocline temperatures by 5 degrees.

[53] The Mg/Ca-derived temperatures derived for *N. dutertrei* suggest that this species is not accurately reflecting changes in temperature but is instead recording changes in preservation/dissolution. Based on the oxygen isotope gradient between the surface and deep species, the stratification was probably greater during the deglacial and LGM. As a result, we caution the use of *N. dutertrei* for thermocline temperature reconstructions or taking the offset in Mg/Ca between *N. dutertrei* and a surface dwelling species as solely reflective of upper water column temperature stratification. *N. dutertrei* Mg/Ca thermometry should be restricted to periods of time when either preservation is similar to modern or when the preservation history can be estimated by another means (e.g., foraminiferal fragmentation [*Mekik et al.*, 2002]). When preservation changes are large and variations in the carbonate ion concentration are not taken into account,

the temperature estimated using *N. dutertrei* Mg/Ca ratios might be inaccurately high. The results also suggest that the Mg/Ca ratios of *N. dutertrei* could be used to quantify the change in the carbonate ion concentration that coincides with deglacial preservation 'spikes' [*Fehrenbacher et al.*, 2007], even when bioturbation may have attenuated the signal.

[54] **Acknowledgments.** We thank Dan McCorkle of Woods Hole Oceanographic Institute for providing samples from the Ontong Java Plateau. We thank Tom Guilderson of Laurence Livermore National Laboratory for assistance with the radiocarbon analysis. We thank David Lea and Mary Jane Coombs for providing the *G. sacculifer* data from core MW91-9 48GGC. We also thank Georges Paradis, Kate Steger, and David Lea for sample analysis at the University of California, Santa Barbara. As part of his undergraduate thesis work, David Levinson counted pteropods in the shallowest three cores. Lauren Camp assisted with sample picking. Discussions with David Archer improved this manuscript.

References

Adkins, J. F., K. McIntyre, and D. P. Schrag (2002), The salinity, temperature, and $\delta^{18}O$ of the glacial deep ocean, *Science*, *298*, 1769–1773, doi:10.1126/science.1076252.

Anand, P., H. Elderfield, and M. H. Conte (2003), Calibration of Mg/Ca thermometry in planktic foraminifera from a sediment trap time series, *Paleoceanography*, *18*(2), 1050, doi:10.1029/2002PA000846.

Anderson, D. M. (2001), Attenuation of millennial-scale events by bioturbation in marine sediments, *Paleoceanography*, *16*, 352–357, doi:10.1029/2000PA000530.

Anderson, D. M., and D. Archer (2002), Glacial-interglacial stability of ocean pH inferred from foraminifer dissolution rates, *Nature*, *416*, 70–73, doi:10.1038/416070a.

Archer, D., S. Emerson, and C. Reimers (1989), Dissolution of calcite in deep-sea sediments: pH and O_2 microelectrode results, *Geochim. Cosmochim. Acta*, *53*(11), 2831–2845, doi:10.1016/0016-7037(89)90161-0.

Archer, D., A. Winguth, D. Lea, and N. Mahowald (2000), What caused the glacial/interglacial atmospheric pCO_2 cycles?, *Rev. Geophys.*, *38*, 159–189, doi:10.1029/1999RG000066.

Archer, D. E. (1991), Equatorial Pacific calcite preservation cycles: Production or dissolution?, *Paleoceanography*, *6*, 561–571, doi:10.1029/91PA01630.

Barker, S., and H. Elderfield (2002), Foraminiferal calcification response to glacial- interglacial changes in atmospheric CO_2, *Science*, *297*, 833–836, doi:10.1126/science.1072815.

Barker, S., W. Broecker, E. Clark, and I. Hajdas (2007), Radiocarbon age offsets of foraminifera resulting from differential dissolution and fragmentation within the sedimentary bioturbated zone, *Paleoceanography*, *22*, PA2205, doi:10.1029/2006PA001354.

Berger, W. H. (1970), Planktic Foraminifera: Selective solution and the lysocline, *Mar. Geol.*, *8*, 111–138, doi:10.1016/0025-3227(70)90001-0.

Berger, W. H. (1977), Deep-sea carbonate and the deglaciation preservation spike in pteropods and foraminifera, *Nature*, *269*, 301–304, doi:10.1038/269301a0.

Berger, W. H. (1978), Deep-sea carbonate: Pteropod distribution and the aragonite compensation depth, *Deep Sea Res.*, *25*, 447–452, doi:10.1016/0146-6291(78)90552-0.

Berger, W. H., and J. S. Killingley (1982), Box cores from the equatorial Pacific: ^{14}C sedimentation rates and benthic mixing, *Mar. Geol.*, *45*, 93–125, doi:10.1016/0025-3227(82)90182-7.

Berger, W. H., T. Bickert, H. Schmidt, and G. Wefer (1983), Quaternary oxygen isotope record of pelagic foraminifers: Site 806, in *Ontong Java Plateau*, *Proc. Ocean Drill. Program Sci. Results*, *130*, 381–395.

Bijma, J., B. Hönisch, and R. E. Zeebe (2002), Impact of the ocean carbonate chemistry on living foraminiferal shell weight: Comment on "Carbonate ion concentration in glacial-age deep waters of the Caribbean Sea" by W. S. Broecker and E. Clark, *Geochem. Geophys. Geosyst.*, *3*(11), 1064, doi:10.1029/2002GC000388.

Billups, K., and D. P. Schrag (2002), Paleotemperatures and ice volume of the past 27 Myr revisted with paired Mg/Ca and $^{18}O/^{16}O$ measurements on benthic foraminifera, *Paleoceanography*, *17*(1), 1003, doi:10.1029/2000PA000567.

Boyle, E. A. (1983), Manganese carbonate overgrowths on foraminifera tests, *Geochim. Cosmochim. Acta*, *47*, 1815–1819, doi:10.1016/0016-7037(83)90029-7.

Boyle, E. A., and L. D. Keigwin (1985), Comparison of Atlantic and Pacific paleochemical records for the last 215,000 years: Changes in deep ocean circulation and chemical inventories, *Earth Planet. Sci. Lett.*, *76*, 135–150, doi:10.1016/0012-821X(85)90154-2.

Broecker, W. S. (1986), Oxygen isotope constraints on surface ocean temperatures, *Quat. Res.*, *26*, 121–134, doi:10.1016/0033-5894(86)90087-6.

Broecker, W. S. (2008), A need to improve reconstructions of the fluctuations in the calcite compensation depth over the course of the Cenozoic, *Paleoceanography*, *23*, PA1204, doi:10.1029/2007PA001456.

Broecker, W. S., and E. Clark (2001a), Glacial-to-Holocene redistribution of carbonate ion in the deep sea, *Science*, *294*, 2152–2155, doi:10.1126/science.1064171.

Broecker, W. S., and E. Clark (2001b), Reevaluation of the $CaCO_3$ size index paleocarbonate ion proxy, *Paleoceanography*, *16*, 669–671, doi:10.1029/2001PA000660.

Broecker, W. S., and E. Clark (2003), Glacial-age deep sea carbonate ion concentrations, *Geochem. Geophys. Geosyst.*, *4*(6), 1047, doi:10.1029/2003GC000506.

Broecker, W. S., K. Matsumoto, E. Clark, I. Hajdas, and G. Bonani (1999), Radiocarbon age differences between coexisting foraminiferal species, *Paleoceanography*, *14*, 431–436, doi:10.1029/1999PA900019.

Broecker, W. S., E. Clark, S. Barker, I. Hajdas, G. Bonani, and E. Moreno (2007), Radiocarbon age of late glacial deep water from the equatorial Pacific, *Paleoceanography*, *22*, PA2206, doi:10.1029/2006PA001359.

Brown, S. J., and H. Elderfield (1996), Variations in Mg/Ca and Sr/Ca ratios of planktic foraminifera caused by postdepositional dissolution: Evidence of shallow Mg-dependent dissolution, *Paleoceanography*, *11*, 543–551, doi:10.1029/96PA01491.

Butzin, M., M. Prange, and G. P. Lohmann (2005), Radiocarbon simulations for the glacial ocean: The effects of wind stress, Southern Ocean sea ice and Heinrich events, *Earth Planet. Sci. Lett.*, *235*, 45–61, doi:10.1016/j.epsl.2005.03.003.

Clark, P. U., A. M. McCabe, A. C. Mix, and A. J. Weaver (2004), Rapid rise of sea level 19,000 years ago and its global implications, *Science*, *304*, 1141–1144, doi:10.1126/science.1094449.

de Garidel-Thoron, T., Y. Rosenthal, L. Beaufort, E. Bard, C. Sonzogni, and A. C. Mix (2007), A multiproxy assessment of the western equatorial Pacific hydrography during the last 30 kyr, *Paleoceanography*, *22*, PA3204, doi:10.1029/2006PA001269.

de Villiers, S. (2003), Dissolution effects on foraminiferal Mg/Ca records of sea surface temperature in the western equatorial Pacific, *Paleoceanography*, *18*(3), 1070, doi:10.1029/2002PA000802.

Dekens, P. S., D. W. Lea, D. K. Pak, and H. J. Spero (2002), Core top calibration of Mg/Ca in tropical foraminifera: Refining paleotemperature estimation, *Geochem. Geophys. Geosyst.*, *3*(4), 1022, doi:10.1029/2001GC000200.

Fairbanks, R. G., and P. H. Wiebe (1980), Foraminifera and chlorophyll maximum: Vertical distribution, seasonal succession, and paleoceanographic significance, *Science*, *209*, 1524–1526, doi:10.1126/science.209.4464.1524.

Fairbanks, R. G., M. Sverdlove, R. Free, P. H. Wiebe, and A. W. H. Bé (1982), Vertical distribution and isotopic fractionation of living planktic foraminifera from the Panama Basin, *Nature*, *298*, 841–844, doi:10.1038/298841a0.

Fairbanks, R. G., et al. (2005), Radiocarbon calibration curve spanning 0 to 50,000 years BP based on paired $^{230}Th/^{234}U/^{238}U$ and ^{14}C dates on pristine corals, *Quat. Sci. Rev.*, *24*, 1781–1796, doi:10.1016/j.quascirev.2005.04.007.

Farmer, E. C., A. Kaplan, P. B. de Menocal, and J. Lynch-Stieglitz (2007), Corroborating ecological depth preferences of planktonic foraminifera in the tropical Atlantic with the stable oxygen isotope ratio of core top specimens, *Paleoceanography*, *22*, PA3205, doi:10.1029/2006PA001361.

Farrell, J. W., and W. L. Prell (1989), Climatic change and $CaCO_3$ preservation: An 800,000 year bathymetric reconstruction from the central equatorial Pacific Ocean, *Paleoceanography*, *4*, 447–466, doi:10.1029/PA004i004p00447.

Fehrenbacher, J., P. A. Martin, and G. Eshel (2006), Glacial deep water carbonate chemistry inferred from foraminiferal Mg/Ca: A case study from the western tropical Atlantic, *Geochem. Geophys. Geosyst.*, *7*, Q09P16, doi:10.1029/2005GC001156.

Fehrenbacher, J., P. A. Martin, and G. Eshel (2007), Deep Pacific carbonate chemistry during the LGM and deglaciation: Reconstructing ΔCO_3^{2-} using foraminiferal Mg/Ca ratios, *Eos Trans. AGU*, *88*(52), Fall Meet. Suppl., Abstract PP43E-07.

Galbraith, E. D., S. L. Jaccard, T. F. Pedersen, D. M. Sigman, G. H. Haug, M. Cook, J. R. Southon, and R. Francois (2007), Carbon dioxide release from the North Pacific abyss during the last deglaciation, *Nature*, *449*, 890–893, doi:10.1038/nature06227.

Ganssen, G. M., S. R. Troelstra, K. van der Borg, and A. M. F. de Jong (1991), Late Quaternary Pteropod Preservation in eastern North Atlantic Sediments in relation to changing climate, *Radiocarbon*, *33*(3), 277–282.

Hales, B. (2003), Respiration, dissolution, and the lysocline, *Paleoceanography*, *18*(4), 1099, doi:10.1029/2003PA000915.

Hastings, D. W., A. Russell, and S. R. Emerson (1998), Foraminiferal magnesium in *Globeriginoides sacculifer* as a paleotemperature proxy, *Paleoceanography*, *13*, 161–169, doi:10.1029/97PA03147.

Herguera, J. C. (1994), Nutrient, mixing and export indices: A 250 Kyr paleoproductivity record from the western equatorial Pacific, in *Carbon Cycling in the Glacial Ocean: Constraints on the Ocean's Role in Global Change*, *NATO ASI Ser., Ser. I*, vol. 17, edited by R. Zahn et al., pp. 481–519, Springer, Berlin.

Herguera, J. C., E. Jansen, and W. H. Berger (1992), Evidence for a bathyal front at 2000-M depth in the glacial Pacific, based on a depth transect on Ontong Java Plateau, *Paleoceanography*, *7*, 273–288, doi:10.1029/92PA00869.

Higgins, S. M., W. Broecker, R. Anderson, D. C. McCorkle, and D. Timothy (1999), Enhanced Sedimentation along the equator in the western Pacific, *Geophys. Res. Lett.*, *26*(23), 3489–3492, doi:10.1029/1999GL008331.

Hönisch, B., and N. G. Hemming (2005), Surface ocean pH response to variations in pCO_2 through two full glacial cycles, *Earth Planet. Sci. Lett.*, *236*, 305–314, doi:10.1016/j.epsl.2005.04.027.

Jahnke, R. A., D. B. Craven, and J. F. Gaillard (1994), The influence of organic-matter diagenesis on $CaCO_2$ dissolution at the deep-sea floor, *Geochim. Cosmochim. Acta*, *58*(13), 2799–2809, doi:10.1016/0016-7037(94)90115-5.

Katz, A. (1973), The interaction of magnesium with calcite during crystal growth at 25–90°C and one atmosphere, *Geochim. Cosmochim. Acta*, *37*, 1563–1586, doi:10.1016/0016-7037(73)90091-4.

Keigwin, L. (1998), Glacial-age hydrography of the far northwest Pacific Ocean, *Paleoceanography*, *13*, 323–339, doi:10.1029/98PA00874.

Labeyrie, L. D., J. C. Duplessy, J. Duprat, A. Juilletleclerc, J. Moyes, E. Michel, N. Kallel, and N. J. Shackleton (1992), Changes in the vertial structure of the North Atlantic Ocean between glacial and modern times, *Quat. Sci. Rev.*, *11*, 401–413, doi:10.1016/0277-3791(92)90022-Z.

Lalli, C. M., and R. W. Gilmer (1989), *Pelagic Snails: The Biology of Holoplanktic Gastropod Mollusks*, 276 pp., Stanford Univ. Press, Stanford, Calif.

Lambeck, K., and J. Chappell (2001), Sea level change through the last glacial cycle, *Science*, *292*, 679–686, doi:10.1126/science.1059549.

Lea, D. W., and P. A. Martin (1996), A rapid mass spectrometric method for the simultaneous analysis of barium, cadmium, and strontium in foraminifera shells, *Geochim. Cosmochim. Acta*, *60*, 3143–3149, doi:10.1016/0016-7037(96)00184-6.

Lea, D. W., T. A. Mashiotta, and H. J. Spero (1999), Controls on magnesium and strontium uptake in planktonic foraminifera determined by live culturing, *Geochim. Cosmochim. Acta*, *63*, 2369–2379, doi:10.1016/S0016-7037(99)00197-0.

Lea, D. W., D. K. Pak, and H. J. Spero (2000), Climate impact of late quaternary equatorial pacific sea surface temperature variations, *Science*, *289*, 1719–1724, doi:10.1126/science.289.5485.1719.

Levitus, S., and T. P. Boyer (1994), *World Ocean Atlas 1994*, vol. 2, *Oxygen, NOAA Atlas NESDIS*, vol. 2, 202 pp., NOAA, Silver Spring, Md.

Marchitto, T. M., J. Lynch-Stieglitz, and S. R. Hemming (2005), Deep Pacific $CaCO_3$ compensation and glacial-interglacial atmospheric CO_2, *Earth Planet. Sci. Lett.*, *231*, 317–336, doi:10.1016/j.epsl.2004.12.024.

Marchitto, T. M., S. J. Lehman, J. D. Ortiz, J. Flückiger, and A. van Geen (2007), Marine radiocarbon evidence for the mechanism of deglacial atmospheric CO_2 rise, *Science*, *8*, 1456–1459, doi:10.1126/science.1138679.

Martin, P. A., and D. W. Lea (2002), A simple evaluation of cleaning procedures on fossil benthic foraminiferal Mg/Ca, *Geochem. Geophys. Geosyst.*, *3*(10), 8401, doi:10.1029/2001GC000280.

Martinet, J. I., P. D. Deckker, and A. R. Chivas (1997), New estimates for salinity changes in the Western Pacific Warm Pool during the Last Glacial Maximum: Oxygen-isotope evidence, *Mar. Micropaleontol.*, *32*, 311–340, doi:10.1016/S0377-8398(97)00029-7.

Mashiotta, T. A., D. W. Lea, and H. J. Spero (1999), Glacial-interglacial changes in subantarctic sea surface temperature and δ^{18}O-water using foraminiferal Mg, *Earth Planet. Sci. Lett.*, *170*, 417–432, doi:10.1016/S0012-821X(99)00116-8.

Matsumoto, K., T. Oba, J. Lynch-Stieglitz, and H. Yamamoto (2002), Interior hydrography and circulation of the glacial Pacific Ocean, *Quat. Sci. Rev.*, *21*, 1693–1704, doi:10.1016/S0277-3791(01)00142-1.

McConnell, M. C., and R. C. Thunell (2005), Calibration of the planktonic foraminiferal Mg/Ca paleothermometer: Sediment trap results from the Guaymas Basin, Gulf of California, *Paleoceanography*, *20*, PA2016, doi:10.1029/2004PA001077.

McKenna, V. S., and W. L. Prell (2004), Calibration of the Mg/Ca of *Globorotalia truncatulinoides* (R) for the reconstruction of marine temperature gradients, *Paleoceanography*, *19*, PA2006, doi:10.1029/2000PA000604.

Mekik, F. A., P. W. Loubere, and D. E. Archer (2002), Organic carbon flux and organic carbon to calcite flux ratio recorded in deep-sea carbonates: Demonstration and a new proxy, *Global Biogeochem. Cycles*, *16*(3), 1052, doi:10.1029/2001GB001634.

Melkert, M. J., G. Ganssen, W. Helder, and S. R. Troelstra (1992), Episodic preservation of pteropod oozes in the deep Northeast Atlantic Ocean: Climatic change and hydrothermal activity, *Mar. Geol.*, *103*, 407–422, doi:10.1016/0025-3227(92)90029-H.

Monnin, E., A. Indermühle, A. Dällenbach, J. Flückiger, B. Stauffer, T. F. Stocker, D. Raynaud, and J.-M. Barnola (2001), Atmospheric CO_2 concentrations over the last glacial termination, *Science*, *291*, 112–114, doi:10.1126/science.291.5501.112.

Montenegro, A., M. Eby, J. O. Kaplan, K. J. Meissner, and A. J. Weaver (2006), Carbon storage on exposed continental shelves during the glacial-interglacial transition, *Geophys. Res. Lett.*, *33*, L08703, doi:10.1029/2005GL025480.

Nürnberg, D., and J. Groeneveld (2006), Pleistocene variability of the Subtropical Convergence at East Tasman Plateau: Evidence from planktonic foraminiferal Mg/Ca (ODP Site 1172A), *Geochem. Geophys. Geosyst.*, *7*, Q04P11, doi:10.1029/2005GC000984.

Nürnberg, D., J. Bijma, and C. Hemleben (1996), Assessing the reliability of magnesium in foraminiferal calcite as a proxy for water mass temperatures, *Geochim. Cosmochim. Acta*, *60*, 803–814, doi:10.1016/0016-7037(95)00446-7.

Oomori, T., H. Kaneshima, Y. Maezato, and Y. Kitano (1987), Distribution coefficient of magnesium ions between calcite and solution at 10–50°C, *Mar. Chem.*, *20*, 327–336, doi:10.1016/0304-4203(87)90066-1.

Peng, T.-H., and W. S. Broecker (1984), The impacts of bioturbation on the age difference between benthic and planktonic foraminifera in deep sea sediments, *Nucl. Instrum. Methods Phys. Res., Sect. B*, *5*, 346–352, doi:10.1016/0168-583X(84)90540-8.

Peterson, M. N. A. (1966), Calcite: Rates of dissolution in a vertical profile in the central Pacific, *Science*, *154*, 1542–1544, doi:10.1126/science.154.3756.1542.

Regenberg, M., D. Nürnberg, S. Steph, J. Groeneveld, D. Garbe-Schönberg, R. Tiedemann, and W.-C. Dullo (2006), Assessing the effect of dissolution on planktonic foraminiferal Mg/Ca ratios: Evidence from Caribbean core tops, *Geochem. Geophys. Geosyst.*, *7*, Q07P15, doi:10.1029/2005GC001019.

Rosenthal, Y., and G. P. Lohmann (2002), Accurate estimation of sea surface temperatures using dissolution-corrected calibrations for Mg/Ca paleothermometry, *Paleoceanography*, *17*(3), 1044, doi:10.1029/2001PA000749.

Sarmiento, J. L., and N. Gruber (2006), *Ocean Biogeochemical Dynamics*, 526 pp., Princeton Univ. Press, Princeton, N. J.

Shackleton, N. J., and N. D. Opdyke (1977), Oxygen isotopes and paleomagnetic evidence for early Northern Hemisphere glaciation, *Nature*, *270*, 216–219, doi:10.1038/270216a0.

Shackleton, N. J., J.-C. Duplessy, M. Arnold, P. Maurice, M. A. Hall, and J. Cartlidge (1988), Radiocarbon age of last glacial Pacific deep water, *Nature*, *335*, 708–711, doi:10.1038/335708a0.

Spero, H. J., K. M. Mielke, E. M. Kalve, D. W. Lea, and D. K. Pak (2003), Multispecies approach to reconstruct eastern equatorial Pacific thermocline hydrography during the past 360 kyr, *Paleoceanography*, *18*(1), 1022, doi:10.1029/2002PA000814.

van der Spoel, S., and R. P. Heyman (1983), *A Comparative Atlas of Zooplankton: Biological Patterns in the Oceans*, 186 pp., Springer, Berlin.

Wu, G., M. K. Yasuda, and W. H. Berger (1991), Late Pleistocene carbonate stratigraphy on Ontong-Java Plateau in the western equatorial Pacific, *Mar. Geol.*, *99*, 135–150, doi:10.1016/0025-3227(91)90087-K.

Yu, J. M., and H. Elderfield (2007), Benthic foraminiferal B/Ca ratios reflect deep water carbonate saturation state, *Earth Planet. Sci. Lett.*, *258*, 73–86, doi:10.1016/j.epsl.2007.03.025.

Zeebe, R. E., and D. Wolf-Gladrow (2001), *CO_2 in Seawater: Equilibrium, Kinetics, Isotopes*, *Elsevier Oceanogr. Ser.*, vol. 65, 360 pp., Elsevier Sci., Amsterdam.

J. Fehrenbacher and P. Martin, Department of Geophysical Sciences, University of Chicago, 5734 S. Ellis Ave., Chicago, IL 60637, USA. (jsf1@uchicago.edu)